

We are IntechOpen, the world's leading publisher of Open Access books Built by scientists, for scientists

6,900

Open access books available

186,000

International authors and editors

200M

Downloads

Our authors are among the

154

Countries delivered to

TOP 1%

most cited scientists

12.2%

Contributors from top 500 universities



WEB OF SCIENCE™

Selection of our books indexed in the Book Citation Index
in Web of Science™ Core Collection (BKCI)

Interested in publishing with us?
Contact book.department@intechopen.com

Numbers displayed above are based on latest data collected.
For more information visit www.intechopen.com



Application of Quantum Mechanics for Computing the Vibrational Spectra of Nitrogen Complexes in Silicon Nanomaterials

Faouzia Sahtout Karoui¹ and Abdennaceur Karoui²

¹*Department of Computer Science, ISCAE,
University of Manouba, Manouba*

²*Department of Natural Science and Mathematics,
Shaw University, Raleigh NC*

¹*Tunisia*

²*USA*

1. Introduction

Nitrogen is a key dopant in silicon for modern electronics including nanoscale devices and third generation solar cells. Even at concentration levels as low as 10^{15} cm^{-3} nitrogen doping can change drastically the physical properties of silicon wafers. For instance, large Czochralski silicon (CZ Si) wafers, as well as float zone silicon (FZ Si) wafers for photovoltaic applications benefit from nitrogen in silicon by increasing wafer toughness. An exceptional hardening due to nitrogen doping enabled the growth of wider silicon crystals, in excess of 300 mm in diameter. Nitrogen doped silicon appeared tougher than its oxygen doped counterpart, which enabled thinner and lighter wafers, thus easier to handle. The hardness is induced by dislocation locking effect (Sumino et al., 1983; Chiou et al., 1984; Abe et al., 1984; Murphy et al., 2006), and an increase of the density of as-grown precipitates which originates from nitrogen-oxygen clusters (Karoui et al., 2004; Karoui & Rozgonyi, 2004; Nakai et al., 2001; Karoui et al., 2002). Nitrogen interacts with point defects such as Si vacancy (V) or Si self-interstitial (I), as well as light impurities affecting the formation of micro-defects, thereby significantly reducing swirl defects as well as vacancy related defects known as D-defects, COPs and voids, and improving the gate oxide integrity (GOI) (von Ammon et al., 1996; Tamatsuka et al., 1999; Ikari et al., 1999). Nitrogen also dramatically enhances oxygen precipitation by interacting with oxygen, achieving strong gettering of metallic impurities in the bulk (Ikari et al., 1999; von Ammon et al., 2001; Shimura & Hockett, 1986; Sun et al., 1992; Aihara et al., 2000). Fourier Transform Infrared Spectroscopy (FTIR) has been extensively used to identify the atomic structure of N-related defects and to determine nitrogen concentration in nitrogen doped FZ (N-FZ) and CZ (N-CZ) Si wafers (Stein, 1983, 1986; Wagner, 1988; Qi et al., 1991; Yang et al., 1998; Qi et al., 1992). FTIR measurements on N-FZ Si wafers shows that 80% of nitrogen atoms are paired (N-pairs) and bonded to silicon at concentration much larger than the solid solubility limit (Stein, 1983). Most nitrogen atoms are coupled by pair and

are fully coordinated with the Si atoms removing any electrical activity (Brower, 1982; Stein, 1987). The possible atomic structures for a N-pairs is either in interstitial split arrangement as suggested by Jones et al. (Jones et al., 1994), or in substitutional position, occupying either a vacancy (V) or a divacancy (V_2), forming nitrogen-vacancy (N-V) complexes (Stein, 1983, 1985). N-V complexes have been identified by DLTS measurement (Fuma et al., 1996), platinum diffusion (Quast et al., 2000) and positron annihilation (Shaik Adam et al., 2001).

As shown in Table 1, the FTIR absorption bands 771 cm^{-1} , 967 cm^{-1} at low temperature ($< 15\text{ K}$) and 766 cm^{-1} , 963 cm^{-1} at room temperature (RT) relate to the localized modes of N-pairs (Stein, 1983; Wagner, 1988; Qi et al., 1991). Two additional FTIR lines, 551 cm^{-1} and 653 cm^{-1} (RT), have been detected after laser annealing of N-implanted FZ Si and have been attributed to N substitutional (Stein, 1985). The absorption coefficient of line 963 cm^{-1} is often used in the calibration curve derived by Itoh et al (Itoh et al., 1985) to measure nitrogen concentration in N-FZ and N-CZ Si wafers: $(1.83 \pm 0.24) \times 10^{17} \times \alpha_{963}\text{ at/cm}^{-3}$.

In N-CZ Si or O-rich N-FZ Si, some of the grown-in N-pairs interact with oxygen forming nitrogen-oxygen or nitrogen-vacancy-oxygen complexes (that we will refer later as N-O complex) hence, reducing the number of N-N centers (Stein, 1986; Wagner, 1988; Qi et al., 1991; Yang et al., 1998; Qi et al., 1992). N-O complexes form between $400\text{ }^\circ\text{C}$ and $700\text{ }^\circ\text{C}$. Beyond $700\text{ }^\circ\text{C}$ these complexes dissociate, emitting the oxygen interstitial atom and leaving the N-pair intact. During subsequent cooling the N-O complexes form again (Wagner, 1988; Qi et al., 1991; Qi et al., 1992; Berg Rasmussen et al., 1996). Both N-N and N-O complexes FTIR response anneal out above $1000\text{ }^\circ\text{C}$. N-O complexes are believed to strongly control the mechanisms of formation of oxygen precipitates and voids in N-doped silicon (Karoui et al., 2004; Karoui & Rozgonyi, 2004; Nakai et al., 2001; Karoui et al., 2002; Von Ammon et al., 2001; Shimura & Hockett, 1986; Stein, 1986; Hara et al., 1989; Rozgonyi et al., 2002). As shown in Table 1, the formation of N-O defects results in several additional infrared absorption bands (Wagner, 1988; Qi et al., 1991; Qi et al., 1992). FTIR absorption lines for N-O defects (at $T < 15\text{ K}$) are 806 , 815 , 1000 , 1021 , and 1031 cm^{-1} . An additional weak line at 739 cm^{-1} has been observed at low temperature in FZ Si samples implanted with nitrogen and oxygen (Berg Rasmussen et al., 1996). The occurrence of these additional infrared (IR) lines affects the measurement of nitrogen concentration in N-CZ Si. The calibration relationship derived by Itoh has been revised by Qi et al (Qi et al., 1992) based on FTIR measurements as follow: $(1.83 \pm 0.24) \times 10^{17} \times (\alpha_{963} + 1.4\alpha_{801})\text{ at/cm}^{-3}$ (300 K) which take into consideration the N-O complexes to whose have been assigned the 801 cm^{-1} absorption line. Despite the technological importance of N-doped Si, little is known about the atomistic structure of N-O complexes often resulting in an inaccurate evaluation of the nitrogen content in silicon. The mechanisms by which nitrogen affects O-precipitation and vacancy aggregation in N-doped silicon remain unclear and direct experimental evidence are still needed. Although, several papers report on the electronic and atomic structure of N-pairs complexes (Jones et al., 1994; Ewels, C., 1997; Sawada & Kawakami, 2000; Kageshima & al., 2000; Goss et al., 2003; Karoui et al., 2003), theoretical studies on N-O complexes atomic structure, stability and vibrational spectra remain scarce (Ewels, C., 1997). Few of them report on the vibrational spectra of N-pair (Ewels, C., 1997; Goss et al., 2003; Jones et al., 1994).

Studying the atomic structure and vibrational spectra of nitrogen-oxygen-vacancy complexes will help us to comprehend how nitrogen, oxygen, and vacancies interact, and how nitrogen effects oxygen precipitation and void formation during crystal growth and

wafer processing. Therefore, to correctly assess nitrogen concentration in N-doped Si crystals. In the present work, we have investigated the formation energy and vibrational spectra of several structures of major grown-in nitrogen-vacancy-oxygen, using quantum mechanics Density Functional Theory (DFT) as implemented in DMol³ package (Delley, 1990; 2000) and, the semi-empirical Modified Neglect of Diatomic Overlap Parametric Method (MNDO) in the restricted Hartree-Fock approximation (UniChem; Dewar et al., 1985). We will start by presenting the theory behind the quantum mechanics computation of vibrational spectra (Bernath, 1995; Harris & Bertolucci, 1985; Atkins & Friedman, 2011). Then we will detail our study followed by results and discussion.

| | FTIR Measurement (cm ⁻¹) | |
|--------|--------------------------------------|---------------------------|
| | <i>T</i> < 15K | <i>RT</i> |
| N-pair | 771, 967 (551, 653, 782, 790)* | 766, 963 |
| N-O | 806, 815, 1000, 1021, 1031 739* | 801, 810, 996, 1018, 1026 |

* Detected in N-FZ implanted wafers.

Table 1. Measured FTIR spectra for N-N and N-O defects (Stein, 1983; Wagner, 1988; Qi et al., 1991; Qi et al., 1992).

2. Experimental measurement of vibrational spectra

Spectroscopy is the study of the interaction of electromagnetic radiation with matter. Molecules, consisting of electrically charged nuclei and electrons, may interact with the oscillating electric and magnetic fields of light and absorb the energy carried by the light. The molecules does not interact with all light that comes its way, but only with light that carries the right amount of energy to promote the molecule from one discret energy level to another. The light can be absorbed and a ground state molecule can be promoted to its first excited vibrational state. When this happen we say that the molecule has made a transition between the ground state and the first excited vibrational state.

Vibrational spectra are measured by two different techniques, *Infrared (IR) spectroscopy* and *Raman spectroscopy*. In *IR spectroscopy*, the infrared spectrum of a sample is recorded by passing a beam of infrared light through the sample. When the frequency of the IR is the same as the vibrational frequency of a bond, absorption occurs. Examination of the transmitted light reveals how much energy was absorbed at each frequency (or wavelength). This can be achieved by scanning the wavelength range using a monochromator. Alternatively, the whole wavelength range is measured at once using a Fourier transform instrument, hence the name of Fourier Transform Infrared Spectroscopy (FTIR). Then, a transmittance or absorbance spectrum is generated using a dedicated procedure. Analysis of the position, shape and intensity of peaks in this spectrum reveals details about the molecular structure of the sample. At frequencies corresponding to vibrational energies of the sample, some light is absorbed and less light is transmitted than at frequencies which do not correspond to vibrationals energies of the molecule. In order to compensate for absorption and scattering of the light by the sample cell, the incident light is split into two beams, one of which goes through the sample, and the other is passed through

a reference cell. Transmittance is then defined as I_s/I_r where I_s is the intensity of light passing through the sample cell, and I_r is the intensity of light passing through the reference cell.

In *Raman spectroscopy* we do not observe transmitted light but light scattered by the sample. The scattered light may be observed from any convenient direction with respect to the incident light. Light of a single frequency, monochromatic light, must be used for a Raman experiment. This phenomenon in which light of frequency ν_0 is scattered in all directions is called Rayleigh scattering. A very small fraction of the scattered light is not of frequency ν_0 . The process which produce light of frequency other than ν_0 is called Raman scattering. The amount of light of frequency less than ν_0 is much greater than that with frequency higher than ν_0 . The former scattered light radiation is called Stokes radiation and the latter is called anti-stokes radiation. In Raman spectroscopy, light of greater value than infrared frequencies is used and we measure the difference between the frequency of the incident light and the one of the Raman scattered light. The molecular vibrations stimulated in the Raman process are not necessarily the same as those excited by the absorption of infrared light. Therefore, the IR and Raman spectra will usually look different and will complement each other.

What exactly happens at a molecular level?

Infrared Spectroscopy: Infrared absorption spectroscopy deals with vibrations of chemical bonds. Light of infrared frequencies can generally promote molecules from one vibrational energy level to another, which allows characterization of atomic bondings and enables identification of the molecule composition and its atomic structure. These capabilities make the IR spectroscopy a powerful tool. Only photons that carry the right amount of energy promote the molecule from one discrete energy level to another.

First we need to describe the permanent dipole moment of a molecule. If two particles of charges $+q$ and $-q$ are separated by a distance r , the permanent electric dipole moment, μ , is given by:

$$\mu = qr \quad (1)$$

Polyatomic molecules with a center of inversion will not have a dipole moment whereas noncentrosymmetric molecules will usually have one. If we consider a heteronuclear diatomic molecule vibrating at a particular frequency, the molecular dipole moment also oscillates about its equilibrium as the two atoms move back and forth. This oscillating dipole can absorb energy from an oscillating electric field only if the field oscillates at the same frequency. The absorption of energy from the light wave by the oscillating permanent dipole is a molecular explanation of IR spectroscopy.

Raman spectroscopy: If a molecule is placed in an electric field, f , a dipole moment, μ_{ind} , is induced in the molecule because the nuclei are attracted toward the negative pole of field, and the electrons are attracted the opposite way. The induced dipole moment is proportional to the field strength α , which is called the *polarizability* of the molecule:

$$\mu_{\text{ind}} = \alpha f \quad (2)$$

All atoms and molecules will have non-zero polarizability even if they have no permanent dipole moment. A light wave electric field oscillates at a certain point in space according to the equation:

$$f = f_0 \cos 2\pi \nu t \quad (3)$$

where f_0 is the maximum value of the field, ν the frequency, and t is time. The induced dipole moment in the oscillating field is:

$$\mu_{\text{ind}} = \alpha f_0 \cos 2\pi \nu t \quad (4)$$

α varies at the natural vibrational frequency of the bond:

$$\alpha = \alpha_0 + (\Delta\alpha) \cos 2\pi \nu_0 t \quad (5)$$

where α_0 is the equilibrium polarizability, $\Delta\alpha$ is its maximum variation, and ν_0 is the natural vibrational frequency. The induced dipole moment is then:

$$\mu_{\text{ind}} = \alpha_0 f_0 \cos 2\pi \nu t + (1/2) \Delta\alpha f_0 [\cos 2\pi(\nu + \nu_0)t + \cos 2\pi(\nu - \nu_0)t] \quad (6)$$

Eq. 6 shows that the induced dipole moment will oscillate with components of frequency ν , $\nu - \nu_0$ and $\nu + \nu_0$. The oscillating electric dipole radiates electromagnetic waves of frequency ν (Rayleigh scattering), $\nu - \nu_0$ (Stokes radiation) and $\nu + \nu_0$ (anti-Stokes radiation).

3. Symmetry point groups

3.1 Introduction

Vibrational spectroscopy and molecular orbital theory make extensive use of molecular symmetry. While it is true that most molecules considered as a whole don't possess any symmetry, many molecules do have local symmetry. In many instances, only a region within the molecule i.e. few atoms and its neighbors, needs to be considered to understand the spectroscopic behavior of this region of the molecule. Studying carefully the symmetry of the molecule reduces significantly the number of energy levels one must deal with. The more symmetric the molecule, the fewer different energy levels it has, and the greater degeneracies of those levels. Symmetry is even powerful than that, because it helps us decide which transitions between energy levels are possible. That is to say a molecule may not be able to absorb light even if that light has precisely the correct energy to span two energy levels of the molecule. The symmetries of the states must be compatible in order that the molecule may absorb light. The selection rules which tell us which transitions are possible, will be one of the most important uses of symmetry and will be explained as we proceed.

3.2 Symmetry operations and molecules

Point symmetry groups are groups whose elements are the symmetry operations of molecules. This group have all the properties of a group in mathematics. They are called point groups because the center of mass of the molecule remains unchanged under all symmetry operations and all of the symmetry elements meet at this point. To determine the symmetry point group of a molecule is very important, because all symmetry related properties are dependent on the symmetry point group of the molecule. A symmetry operation is an operation that leaves an object apparently unchanged. Every object has at least one symmetry operation: the *identity*, the operation of doing nothing. To each symmetry operation there corresponds a symmetry element, the point, line, or plane with respect to which the operation is carried. There are five types of symmetry operations that leave the object apparently unchanged and five corresponding types of symmetry element:

E : The *identity operation*, the act of doing nothing. The corresponding symmetry element is the object itself.

C_n : An *n-fold rotation*, the operation, a rotation by $2\pi/n$ around an axis of symmetry.

σ : A reflection in a mirror plane. When the mirror plane includes the principal axis of symmetry, it is termed a *vertical plane* and denoted σ_v . If the principal axis is perpendicular to the mirror plane, then the latter symmetry element is called a *horizontal plane* and denoted σ_h . A *dihedral plane*, σ_d , is a vertical plane that bisects the angle between two C_2 axes that lie perpendicular to the principle axis.

i : An *inversion*, the operation through a center of symmetry. The inversion operation consists of taking each point of an object through its center and out to an equal distance on the other side.

S_n : An *n-fold improper rotation* about an axis of improper rotation. It is a composite operation consisting of an n-fold rotation followed by a horizontal reflection in a plane perpendicular to the n-fold axis. Particular cases are S_1 which is equivalent to a reflection and S_2 is equivalent to an inversion.

Lets consider the group C_{2h} which is, as we will show later, the point group associated with the N_2 molecule in Si. Point group C_{2h} has four members, $\{E, C_2, \sigma_h$ and $i\}$. E is the identity operation which leave the molecule unchanged; C_2 is a n-fold ($n=2$ here) rotation by $2\pi/n$ (180° for C_2) around an axis of symmetry; σ_h is a reflection in a mirror plane (here a plane perpendicular to the principal axis C_2). All the symmetry operations of a molecule as a group can be written in the form of group multiplication table and they obey all the properties of a group. The product of any two operations must be a member of the group. For example the product of two C_2 operations is the identity operation E which is indeed a member of the group. Also $C_2 \cdot \sigma_h = i$, i is also a member of the group. Table 2 shows the complete multiplication table for the point group C_{2h} .

| C_{2h} | E | C_2 | σ_h | i |
|------------|------------|------------|------------|------------|
| E | E | C_2 | σ_h | i |
| C_2 | C_2 | E | i | σ_h |
| σ_h | σ_h | i | E | C_2 |
| i | i | σ_h | C_2 | E |

Table 2. Multiplication Table for the Point Group C_{2h} .

However, to further determine the symmetry properties of molecular orbitals and vibrational modes we need character tables which will be introduced next.

3.3 Characters and character tables

We can use matrices as representations of symmetry operations. Let's consider the symmetry group (C_{2h}) of N_2 defect. Consider a vector $\vec{v}_1 \begin{pmatrix} x_1 \\ y_1 \\ z_1 \end{pmatrix}$, assuming that the principal axis C_2 is the z axis, using matrices representations, \vec{v}_1 will transform as follow through the different operations of the group:

$$\begin{bmatrix} 1 & 0 & 0 \\ 0 & 1 & 0 \\ 0 & 0 & 1 \end{bmatrix} \cdot \begin{bmatrix} x_1 \\ y_1 \\ z_1 \end{bmatrix} = \begin{bmatrix} x_1 \\ y_1 \\ z_1 \end{bmatrix} \quad (7)$$

$$E \cdot \vec{v}_1 = \vec{v}_1 \quad (8)$$

$$\begin{bmatrix} -1 & 0 & 0 \\ 0 & -1 & 0 \\ 0 & 0 & -1 \end{bmatrix} \cdot \begin{bmatrix} x_1 \\ y_1 \\ z_1 \end{bmatrix} = \begin{bmatrix} -x_1 \\ -y_1 \\ -z_1 \end{bmatrix} \quad (9)$$

$$i \cdot \vec{v}_1 = -\vec{v}_1 \quad (10)$$

σ_h leaves the x and y coordinates unchanged but changes z to -z:

$$\begin{bmatrix} 1 & 0 & 0 \\ 0 & 1 & 0 \\ 0 & 0 & -1 \end{bmatrix} \cdot \begin{bmatrix} x_1 \\ y_1 \\ z_1 \end{bmatrix} = \begin{bmatrix} x_1 \\ y_1 \\ -z_1 \end{bmatrix} \quad (11)$$

$$\sigma_h \cdot \vec{v}_1 = -\vec{v}_2 \quad (12)$$

and C_2 which correspond to 180° rotation around the z axis leaves the z coordinate unchanged but changes the x and y coordinates as follow:

$$\begin{bmatrix} \cos\pi & \sin\pi & 0 \\ -\sin\pi & \cos\pi & 0 \\ 0 & 0 & 1 \end{bmatrix} \cdot \begin{bmatrix} x_1 \\ y_1 \\ z_1 \end{bmatrix} = \begin{bmatrix} -1 & 0 & 0 \\ 0 & -1 & 0 \\ 0 & 0 & 1 \end{bmatrix} \cdot \begin{bmatrix} x_1 \\ y_1 \\ z_1 \end{bmatrix} = \begin{bmatrix} -x_1 \\ -y_1 \\ z_1 \end{bmatrix} \quad (13)$$

$$R_0 \cdot \vec{v}_1 = \vec{v}_2 \quad (14)$$

The four matrices form a mathematical group which obeys the same multiplication table as the operations. Therefore, each matrix has an inverse matrix just as each operation of a group has an inverse operation. Using a matrix and its inverse we can perform similarity transformations with matrices:

$$B = Q^{-1} \cdot A \cdot Q \quad (15)$$

A and B are said to be conjugate just as symmetry operations related by similarity transformations are said to be conjugate. Through similarity of transformation, we can define the reducible and irreducible representations of a group. If a matrix representation A can be transferred to block-factored matrix, a matrix composed of blocks (A_1, A_2, A_3) at the diagonal and zero in any other position, by similarity transformation, A is called the reducible representation of the group. If blocks (A_1, A_2, A_3) cannot be further transferred to block-factored matrix through similarity transformation, A_1, A_2, A_3 are called irreducible representations of the group. The sum of the trace of A_1, A_2, A_3 is called the characters of this representation. Reducible representations can be reduced to irreducible representations and irreducible representations cannot be reduced further. The complete list of characters of all possible irreducible representations of a group is called a *character table*. There are only a finite number of irreducible representations for group of finite order. We will see that these tables are of great importance and usefulness when analysing the vibration modes of molecules.

The members of a group can be divided into classes. Two members of a group, P and R, belong to the same class if they are conjugate to each other. As an example, all possible classes associated with the symmetry group $C_{2h}(N_2)$ defect are the following:

- E is in a class by itself since $A^{-1}EA = A^{-1}(EA) = A^{-1}A = E$ for any operation A of the group.
- C_2 : $C_2^{-1}C_2C_2 = C_2^{-1}(C_2C_2) = C_2(E) = C_2$

- $i^{-1}C_2i = i^{-1}(C_2i) = i(\sigma_h) = C_2$
- $\sigma_h^{-1}C_2\sigma_h = \sigma_h^{-1}(C_2\sigma_h) = \sigma_h(i) = C_2$

Hence, for any operation A of the group we have $A^{-1}C_2A = A^{-1}(C_2A) = A^{-1}A = C_2$. In a same way, based on the multiplication Table 2, we can verify that $A^{-1}iA = A^{-1}(iA) = A^{-1}A = i$ and $A^{-1}\sigma_h A = A^{-1}(\sigma_h A) = A^{-1}A = \sigma_h$. Therefore, we have four classes for the group symmetry C_{2h} : $\{E\}$, $\{C_2\}$, $\{i\}$, $\{\sigma_h\}$. Each class correspond to an irreducible representation.

We have as much as irreducible representations as classes of operations in the group. The character of an irreducible representation is the trace, the sum of the diagonal elements, of the matrix representing the irreducible representation. The sum of the traces equal the order of the group. All characters of a group are given in a table, Table 3. This table is divided in several areas. The main part contains the characters. On the left are the *names* of the irreducible representations, known as Mulliken symbols. Conventionally, we use the letters A, B, E, and T (or F in some tables). A and B are one-dimensional. E is two-dimensional and T is three-dimensional. The dimension of an irreducible representation is the dimension of any of its matrices. Since the representation of the operation E is always the identity matrix, the character of E is always the dimension of the irreducible representation. The difference between A and B is that the character under the principal rotational operation, C_n , is always +1 for A and -1 for B representations. The subscript 1,2,3, etc., which may be appear with A, B, E or T can be considered arbitrary label. The subscript *g* (German word *gerade* meaning *even*) means the representation is symmetric with respect to inversion and, the subscript *u* (German word *ungerade* meaning *odd*) means that the representation is antisymmetric to inversion. Any p or f orbital is transformed into minus upon inversion, is therefore a *u* function. A d orbital is transformed into itself upon inversion and is therefore, a *g* function. In a similar way, the superscripts ' and " denote irreducible representations which are respectively, symmetric and antisymmetric with respect to reflection through a horizontal mirror plane. The two columns on the right side of the table contain basis functions for the irreducible representations. The character table for the point group C_{2h} (N_2 defect) is as follow (Bernath, 1995; Harris & Bertolucci, 1985)

| C_{2h} | E | C_2 | i | σ_h | | |
|----------|---|-------|---|------------|------------|---------------------|
| A_g | 1 | 1 | 1 | 1 | R_z | x^2, y^2, z, xy^2 |
| B_g | 1 | 1 | 1 | -1 | R_x, R_y | xz, yz |
| A_u | 1 | -1 | 1 | 1 | z | |
| B_u | 1 | -1 | 1 | -1 | x, y | |

Table 3. Character Table for the Point Group C_{2h} : N_2 Defect.

3.4 Atomic orbitals and symmetry

One-electron wavefunctions in atoms are called *atomic orbitals*. Atomic orbitals with $l=0$ are called s-orbitals, those with $l = 1$ are called p-orbitals, those with $l = 2$ are called d-orbitals, and those with $l = 3$ are called f-orbitals. We are mainly interested here to s- and p-orbitals because the atoms of interest namely nitrogen, oxygen, and Si atoms are bonded to Si neighbors by sp^3 hybrid electron orbital that protrude in a tetrahedral shape. The s-orbitals are spherically symmetrical; the three real orbitals p_x , p_y , p_z have the same double-lobed shape, but are aligned with the x-, y-, and z-axes, respectively; they are shown in Fig. 1.

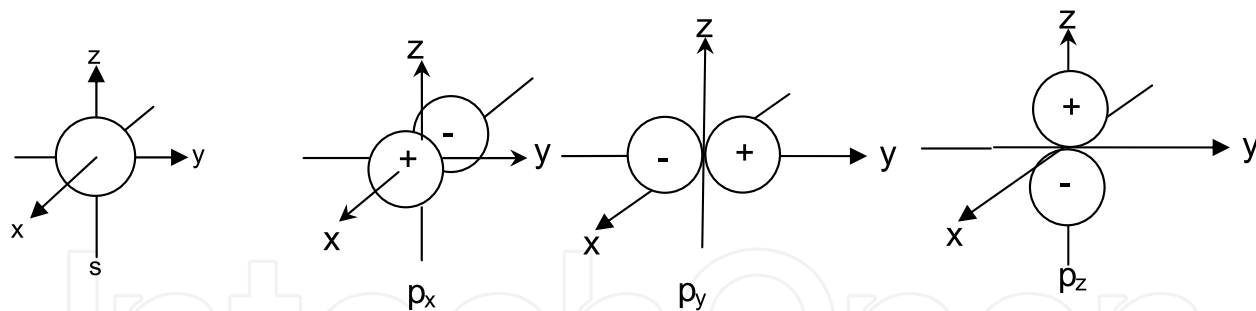


Fig. 1. The s , p_x , p_y , p_z atomic orbitals.

As stated before, the two columns on the right side of the table contain basis functions for the irreducible representations. These basis functions have the same symmetry properties as the atomic orbitals which bear the same names. To understand what a basis function is, let's go back to the matrix representations for the operations of C_{2h} (N_2 defect). The E operation does nothing; the C_2 operation about the z axis leaves the z coordinate of any point unchanged, but changes the x and y coordinates according to R_{θ} ; the σ_h is a reflection in the mirror plane $(x,y) \perp z$ (C_2 axis); and finally the inversion operation i changes each coordinate into minus itself. The atomic orbitals will obey the same multiplication table as the operations, Fig. 2:

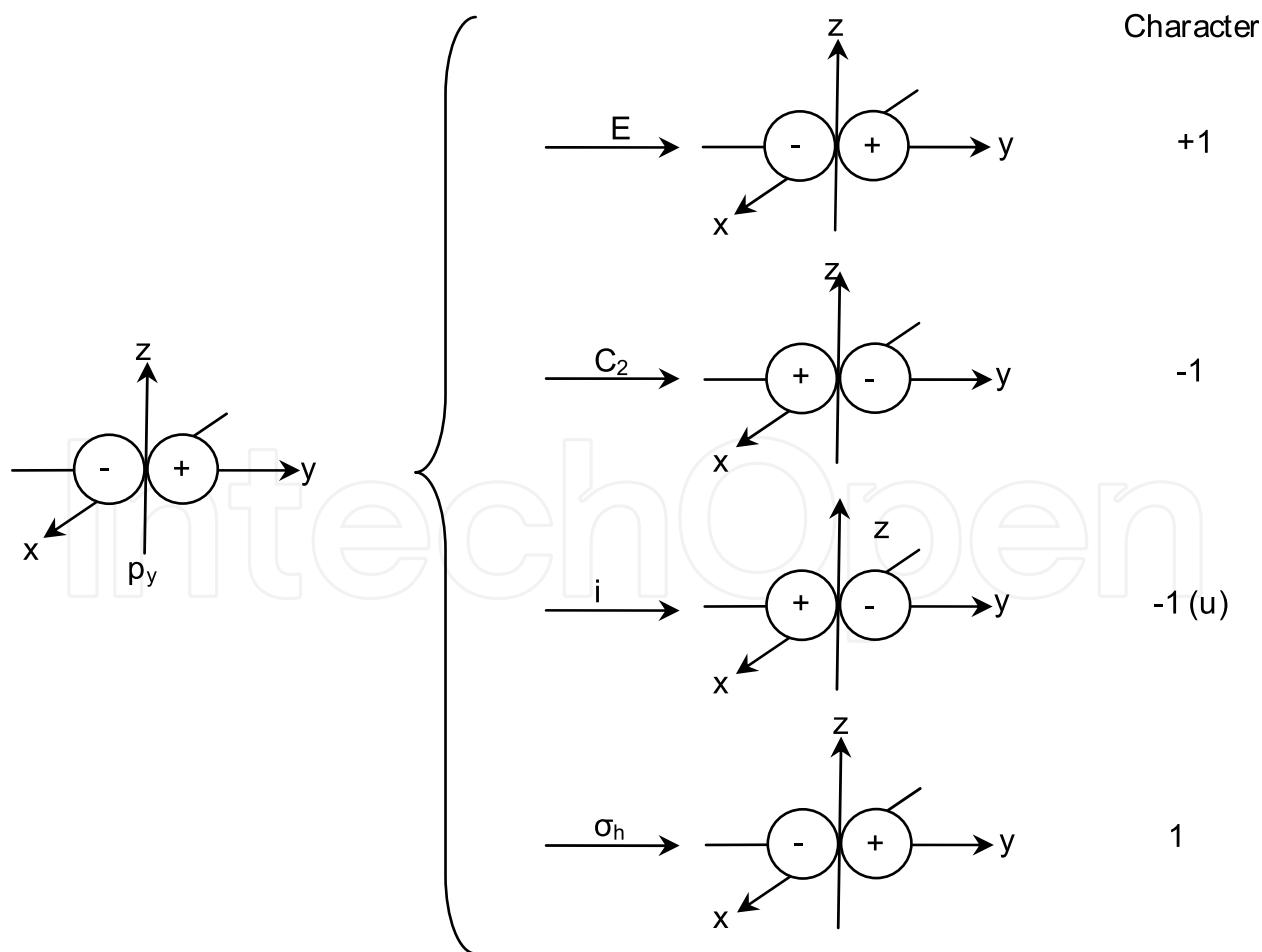


Fig. 2. Orbital p_y through the operation of symmetry point group C_{2h} .

We can see that p_y orbital changes as B_u irreducible representation through the operations of the group $C_{2h} : (E, C_2, i, \sigma_h) : (1, -1, -1, 1) \equiv \{B_u\}$.

4. Vibrational spectroscopy modeling

4.1 Introduction

In IR spectroscopy, molecules are modeled as an assembly of oscillators which interact with the electric and magnetic fields of incident light and absorb energy of incident photons. The total energy of a single molecule, whether in free space or embedded in liquid or solid material, involves different types of molecule motions and behaviors. Hence, the molecule energy is decomposed in: (i) translational energy levels, which are related to the movement of the molecule as a whole. As these levels are very close to each other, they appear continuous, (ii) rotational energy levels, they implicate rotation of the whole molecule, (iii) vibrational energy levels, which are due to the vibration of chemical bonds within the molecule, and (iv) the electronic energy associated to the electrons of the molecule. To better comprehend the vibrational spectroscopy modeling we will start with diatomic molecules and then generalize the model to polyatomic molecules.

4.2 The vibration modeling of diatomic molecules

4.2.1 Introduction

The solution of the Schrödinger equation for a diatomic molecule plays an important role in spectroscopy. In addition, the vibrational spectra of diatomic molecules illustrate most of the fundamental principles which apply to complicated polyatomic molecules. Diatomic molecules can be simulated as shown in Fig. 3. The center of mass of a diatomic is defined such that $m_1 r_1 = m_2 r_2$. The moment of inertia of a system is defined as:

$$I = \sum_i m_i r_i^2 \quad (16)$$

where r_i is the distance of mass m_i from the center of mass. For diatomic molecules,

$$I = \frac{m_1 m_2}{m_1 + m_2} r_e^2 \equiv \mu r_e^2 \quad (17)$$

where

$$\mu \equiv \frac{m_1 m_2}{m_1 + m_2} \quad (18)$$

The quantity μ is called the reduced mass and should not be confused with the dipole moment which has the same symbol.

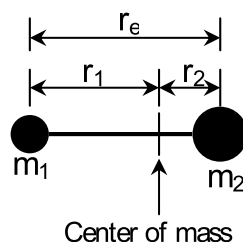


Fig. 3. Model for diatomic molecules.

The molecular potential energy of a diatomic molecule increases if the nuclei are displaced from their equilibrium positions. When the displacement is small, we can express the potential energy as the first few terms of Taylor series:

$$V(x) = V(0) + \left(\frac{dV}{dx}\right)_0 x + \frac{1}{2} \left(\frac{d^2V}{dx^2}\right)_0 x^2 + \frac{1}{6} \left(\frac{d^3V}{dx^3}\right)_0 x^3 + \dots \quad (19)$$

Since we are not interested in the absolute potential energy of the molecule, we can set $V(0) = 0$.

4.2.2 Harmonic oscillation

The harmonic oscillator model is one of the most important models in chemical physics, and has been used extensively in molecular spectroscopy. Provided that the displacement x is small, the terms in Eq. 19 that are higher than second order may be neglected, so we may write

$$V(x) = \frac{1}{2} kx^2 \quad k = \left(\frac{d^2V}{dx^2}\right)_0 \quad (20)$$

This means that the potential energy close to equilibrium is parabolic. It follows that the hamiltonian for the two atoms of masses m_1 and m_2 is

$$H = -\frac{\hbar^2}{2m_1} \frac{d^2}{dx_1^2} - \frac{\hbar^2}{2m_2} \frac{d^2}{dx_2^2} + \frac{1}{2} kx^2 \quad (21)$$

Therefore, when the potential energy depends only on the separation of the particles, the hamiltonian can be expressed as a sum, one term referring to the motion of the center of mass of the system and the other to the relative motion. The former term is of no concern here as it corresponds to the translational motion of the molecule. The latter term is

$$H = -\frac{\hbar^2}{2\mu} \frac{d^2}{dx^2} + \frac{1}{2} kx^2 \quad (22)$$

where μ is the reduced mass.

A hamiltonian with a parabolic potential energy as in Eq. 23, is characteristic of a *harmonic oscillator*. The solutions for the harmonic oscillator is

$$E_\nu = \left(\nu + \frac{1}{2}\right) \hbar\omega \quad \omega = \frac{1}{2\pi} \sqrt{k/\mu} \quad (23)$$

with $\nu = 0, 1, 2, \dots$. These levels lie in a uniform ladder with separation $\hbar\omega$, see Fig. 4. The corresponding wavefunctions are bell-shaped Gaussian functions multiplied by a Hermite polynomial. In the lowest vibrational state ($\nu = 0$), the molecule still has the *zero point energy*, $E_0 = \frac{1}{2} \hbar\omega$. The vibrational spectra of diatomic molecules usually result from excitation from the $\nu = 0$ to the $\nu = 1$ energy levels.

4.2.3 Anharmonic oscillation

The truncation of Taylor expansion of the molecular potential energy in Eq. 20 is only an approximation, and in real molecules the neglected terms are important, particularly for

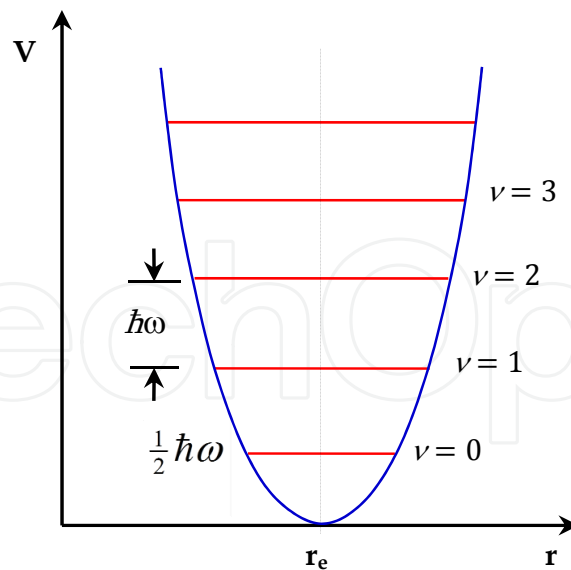


Fig. 4. Harmonic oscillator potential well and energy levels. $V = \frac{1}{2}k(r - r_e)^2$.

large displacements from equilibrium. The typical form of the potential is shown in Fig. 5 and because of high excitations it is less confining than a parabola; the energy levels converge instead of staying uniformly separated. It follows that anharmonic vibration is increasingly important as the degree of vibrational excitation of a molecule is increased. One way for coping with anharmonicities is to solve the Schrodinger equation with a potential energy term that matches the true potential energy over a wide range. One of the most useful approximation function is the *Morse potential* :

$$V(x) = \hbar c D_e (1 - e^{-ax})^2 \quad a = \left(\frac{k}{2\hbar c D_e} \right) \quad (24)$$

The parameter D_e is the depth of the minimum of the curve and $x = r - r_e$ the displacement. At small displacement, the Morse and harmonic oscillator potentials coincide. The quantized energy levels, solution of the Schrodinger equation with the Morse potential are

$$E_v = \left(v + \frac{1}{2} \right) \hbar \omega - \left(v + \frac{1}{2} \right)^2 \hbar \omega x_e \quad (25)$$

with

$$\omega x_e = \frac{a^2 \hbar}{2\mu}$$

The quantity x_e is called the anharmonicity constant. The energy levels at high excitation converge as v becomes large. The ground state of a Morse potential has a zero-point energy of

$$E_0 = \frac{1}{2} \hbar \omega \left(1 - \frac{1}{2} x_e \right) \quad (26)$$

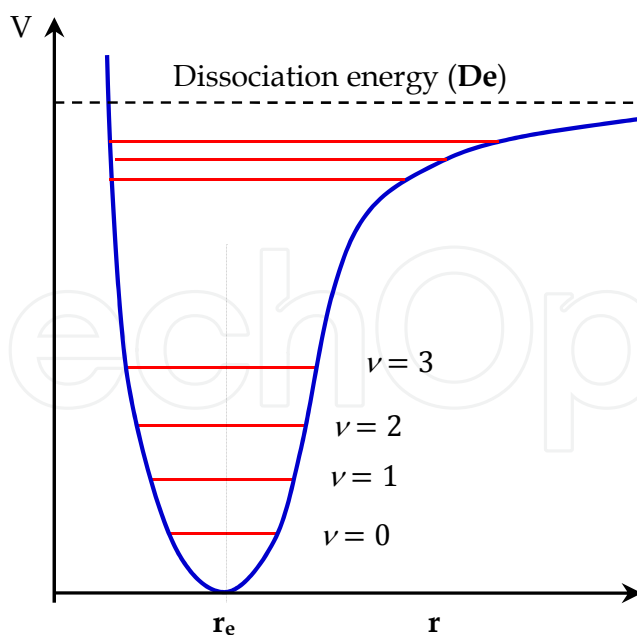


Fig. 5. The Morse potential : $V = \frac{1}{2} \hbar c D_e (1 - e^{-a(r-r_e)})^2$

4.2.4 Vibrational selection rule

The selection rules for the vibrational transition $\nu' \leftarrow \nu$ are based on the electric dipole transition moment. The selection rules for electric-dipole transitions, specify the specific optical transitions that occur based on the examination of dipole moment transitions between the two states of interest. Because the dipole moment μ depends on the bond length R , we can express its variation with displacement of the nuclei from equilibrium as

$$\mu = \mu_0 + \left(\frac{d\mu}{dx} \right)_0 x + \frac{1}{2} \left(\frac{d^2\mu}{dx^2} \right)_0 x^2 + \dots \quad (27)$$

where μ_0 is the dipole moment when the displacement is zero.

To show a vibrational spectrum, a diatomic molecule must have a dipole moment that varies with extension. The selection rule for electric dipole vibrational transitions within the harmonic approximation is $\Delta\nu = \pm 1$.

The selection rule for the observation of vibrational Raman spectra of diatomic molecules is that the molecular polarizability must vary with internuclear separation. The selection rule for vibrational Raman transitions is the same, $\Delta\nu = \pm 1$, as for vibrational absorption and emission because the polarizability, like the electric dipole moment, returns to its initial value once during each oscillation. The transitions with $\Delta\nu = +1$ give rise to the Stokes lines in the spectrum, and those with $\Delta\nu = -1$ give the anti-Stokes lines. Only the Stokes lines are normally observed, because most molecules have $\nu = 0$ initially.

4.3 Vibration of polyatomic molecules

4.3.1 Normal modes of vibration and symmetry

A diatomic molecule possesses a single vibration. Even at absolute zero this vibration occurs because the molecule cannot have less than the zero point energy. Polyatomic molecules undergo much more complex vibrations. However, these motions may be resolved into a

superposition of a limited number of fundamental motions called normal modes of vibration. We are interested in the number, types, and symmetries of these modes.

The motion of a single particle in a three dimensional space can be represented by three coordinates, each one representing a translation of the particle in the x , y , or z direction. The particle is said to have three degrees of freedom. For a diatomic molecule, since we have two particles, the system as a whole has six degrees of freedom. Three are translation in the x , y , or z directions. Two degrees of freedom correspond to rotations about the center of mass. The rotation about the molecular axis of a linear molecule is undefined because it does not represent any change of the nuclear coordinates. Only one vibrational degree of freedom is left, Fig. 6.

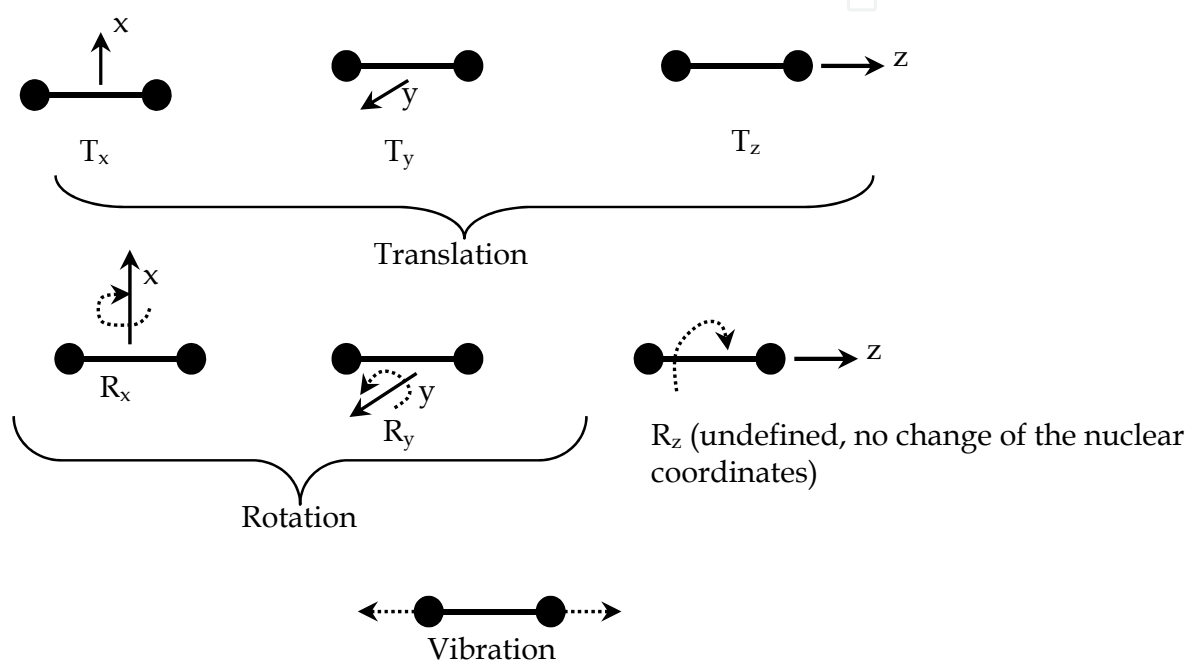


Fig. 6. Degrees of freedom (six) of a diatomic molecule; only one vibration mode ($3 \times 2 - 5 = 1$).

A nonlinear molecular system containing three particles (e.g. water molecule) has nine degrees of freedom. Three translations, three rotations, and three vibrational degrees of freedom. These three kinds of vibration are the three normal modes of vibration of the molecule. In general, a nonlinear molecule with n atoms will have $3n - 6$ modes of vibration; a linear molecule will have $3n - 5$ modes of vibration because there is no rotation about the molecular axis. Within a molecule, atomic displacements occur at the same frequency and in phase. Displacement is measured from the equilibrium atomic separation in the ground state along a normal coordinate. A normal coordinate, q_i , is a single coordinate along which the progress of a single normal mode of vibration can be followed; q_i is a mass-weighted coordinate. The normal coordinates are defined such that the potential energy V and the kinetic energy K of the molecule are as follows (Harris & Bertolucci, 1985)

$$V = (1/2) \sum_i \lambda_i q_i^2 \quad (28)$$

$$K = (1/2) \sum_i (dq_i/dt)^2 \tag{29}$$

where λ_i is a constant. The vibrations that correspond to displacements along these normal coordinates are called the *normal modes* of the molecule. In the harmonic approximation, the ground state vibrational wavefunctions of a molecule is totally symmetric under all symmetry operations of the molecule. The ground state vibrational wavefunctions therefore spans the completely symmetric irreducible representations of the molecular point group.

Each normal mode of vibration will form a basis for an irreducible representation of the point group of the molecule. This key property which connects the symmetry of normal modes of vibration to the symmetry point group of the molecule.

Lets consider the Si₂O molecule which belongs to point group C_{2v}. As we will see subsequently, this molecule is of particular interest to our study. C_{2v} character table is given in Table 4. The operations of the group C_{2v} are (E, C₂, σ_v(xz) and σ'_v(yz)). The three normal modes of vibration of Si₂O are given in Fig. 7 and are noted ν₁, ν₂, ν₃. We are going now to study the effect of each operation of the group on the ν₃ vibration.

| C _{2v} | E | C ₂ | σ _v (xz) | σ' _v (yz) | | |
|-----------------|---|----------------|---------------------|----------------------|-------------------|--|
| A ₁ | 1 | 1 | 1 | 1 | z | x ² , y ² , z ² |
| B ₁ | 1 | 1 | -1 | -1 | R _z | xy |
| A ₂ | 1 | -1 | 1 | -1 | x, R _y | xz |
| B ₂ | 1 | -1 | -1 | +1 | y, R _x | yz |

Table 4. Character Table for the Symmetry Point Group C_{2v} : Si₂O molecule.

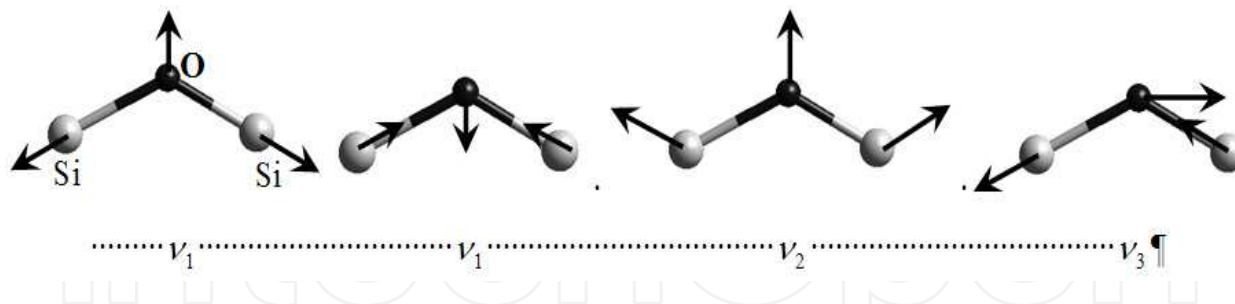


Fig. 7. ν₁ (symmetric stretching, 517 cm⁻¹), ν₂ (symmetric bending, 1203 cm⁻¹), ν₃ (asymmetric stretching, 1136 cm⁻¹) normal modes of Si₂O.^{78,86}

The operation E leaves the ν₃ vibration unchanged so it has the character +1. The C₂ operation changes the direction of motion of each atom when the molecule is vibrating in the normal mode ν₃. Each atom moves in the opposite direction after performing the C₂ operation (Fig. 8). Therefore, the character of C₂ is -1. Similarly, σ_v(xz) changes the direction of motion of the atoms and σ'_v(yz) leaves them unchanged. Hence, they have the character -1 and +1 respectively. In a similar way, we can easily show that ν₁ and ν₂ does not change through all the group operations. This leads us to the characters table given in Table 5 for the vibration modes of the Si₂O molecule.

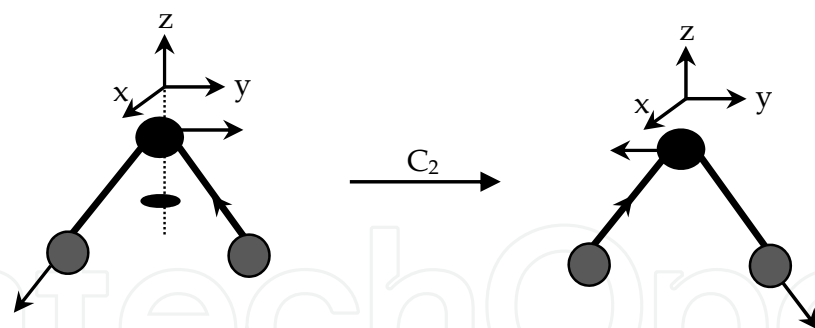


Fig. 8. Application of C_2 operation on the normal mode ν_3 of Si_2O .

| C_{2v} | E | C_2 | $\sigma_v(xz)$ | $\sigma'_v(yz)$ |
|----------|---|-------|----------------|-----------------|
| ν_1 | 1 | 1 | 1 | 1 |
| ν_2 | 1 | 1 | 1 | 1 |
| ν_3 | 1 | -1 | -1 | 1 |

Table 5. Character table for the normal modes of vibration of Si_2O (C_{2v}).

If we look at Table 4 and Table 5 we can see that ν_1 changes as A_1 representation through the operations of the group, ν_2 as A_1 and ν_3 as B_2 . Vibration modes ν_1 and ν_2 are symmetric stretching and symmetric bending modes respectively, while ν_3 is an asymmetric stretching mode. All three normal modes are infrared active because they have the same symmetry as z and y .

4.3.2 Selection rules for polyatomic molecules

Non-zero dipole moment transition corresponds to allowed transition, and vice-versa. At this point, we are interested only in transitions within a given electronic state. The selection rules are derived from the transition matrix by expressing the matrix element in terms of, in a first approximation, the harmonic oscillator wavefunctions. The selection rule for harmonic oscillators are $\Delta\nu = \pm 1$. Each normal mode of vibration shall obey this selection rule within the harmonic approximation. Moreover, electric dipole transitions can occur only for normal modes that correspond to a change in the electric dipole moment of the molecule. The molecular dipole moment depends on an arbitrary displacement as follows:

$$\mu = \mu_0 + \left(\frac{d\mu}{dq_i}\right)_0 q_i + \frac{1}{2} \left(\frac{d^2\mu}{dq_i^2}\right)_0 q_i^2 + \dots \quad (30)$$

where q_i are the normal coordinates.

Since, electric dipole transitions occur only for normal modes that correspond to a change in the electric dipole moment of the molecule, normal modes for which $(\partial\mu/\partial q_i)_0 \neq 0$ are said to be *infrared active* as they can contribute to a vibrational, infrared, absorption, or emission spectrum. Group theory, as shown before, greatly aids the determination of which modes are infrared active.

Normal modes for which the polarizability varies as the atoms are displaced collectively along a normal coordinate i.e. $(\partial\alpha/\partial q_i)_0 \neq 0$, are classified as Raman active as they can contribute to a Raman spectrum.

5. Quantum mechanics computation of the equilibrium structure, energy and vibrational spectra of nitrogen-related complex in nitrogen-doped silicon

5.1 Introduction

In the present work, we have investigated the formation energy and vibrational spectra of several structures of major grown-in nitrogen-vacancy-oxygen, using quantum mechanics Density Functional Theory (DFT) as implemented in DMol³ package and, the semi-empirical Modified Neglect of Diatomic Overlap Parametric Method (MNDO) in the restricted Hartree-Fock approximation. The defects that are of interests are N-pairs structures either in interstitial (N₂) or substitutional positions coupled to a Si vacancy or a divacancy (VN₂ and V₂N₂) and N-O complexes formed by the coupling of these N-N centers with a O_i or an oxygen dimer (O₂). MNDO calculations were solely performed to compute the IR absorption band intensities and electric charges of the IR active LVMs obtained by DMol³-DFT, because not attainable on periodic systems. Performing ab-initio total energy calculations and normal mode analysis require powerful computational resources. Therefore, all our calculations have been carried out on various multiprocessor supercomputers: Origin2400 for COMPASS Force field and Fastructure calculations, IBM SP for the DMol³-DFT calculations and Cray T916 for the MNDO-AM1 calculations.

We have cross-correlated the formation energy, the degree of stability, and the vibrational spectra of each complex in order to precisely identify their structure (Karoui Sahtout & A. Karoui, 2010). Calculated vibrational spectra have been compared to experimental spectra obtained by Fourier-transform infrared spectroscopy.

5.2 Computational method

5.2.1 Chemical reactions and atomic structure of N-pairs and N-O complexes

To simulate the defected crystal structure while preserving the symmetry group of the diamond structure of the host crystal, we built a periodic cubic system consisting of a supercell of 64 silicon atoms with the defect located in its center. All N-defects are in their neutral state. To avoid defect-defect interactions during relaxation, the Si atoms at the boundaries of the supercell were maintained immobile.

The chemical reactions considered in this study to produce N-pairs either in interstitial or substitutional position are shown below:



N_i and N_s are nitrogen atoms in interstitial and substitutional position, respectively, V is a Si vacancy and V₂ a Si divacancy.

The neutral N_2 has a C_{2h} symmetry (Fig. 9) with the axis parallel to $\langle 110 \rangle$ direction, see Fig. 10 (a), and the N-N center sits symmetrically off the bond center, in an anti-parallel

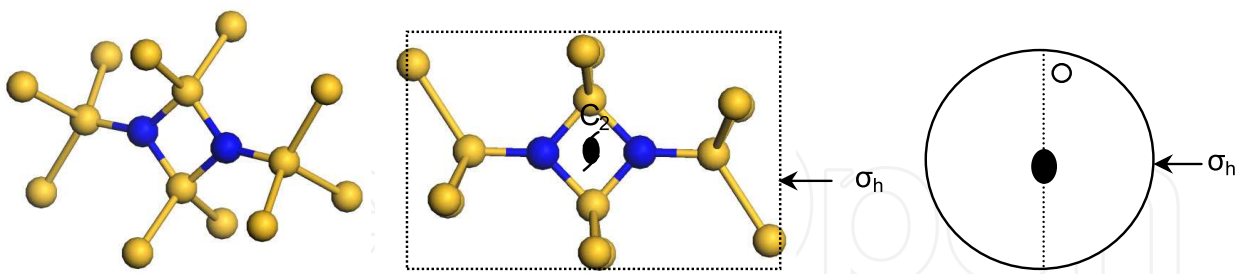


Fig. 9. N_2 Molecule Structure in Si, symmetry point group C_{2h} and stereographic projection.

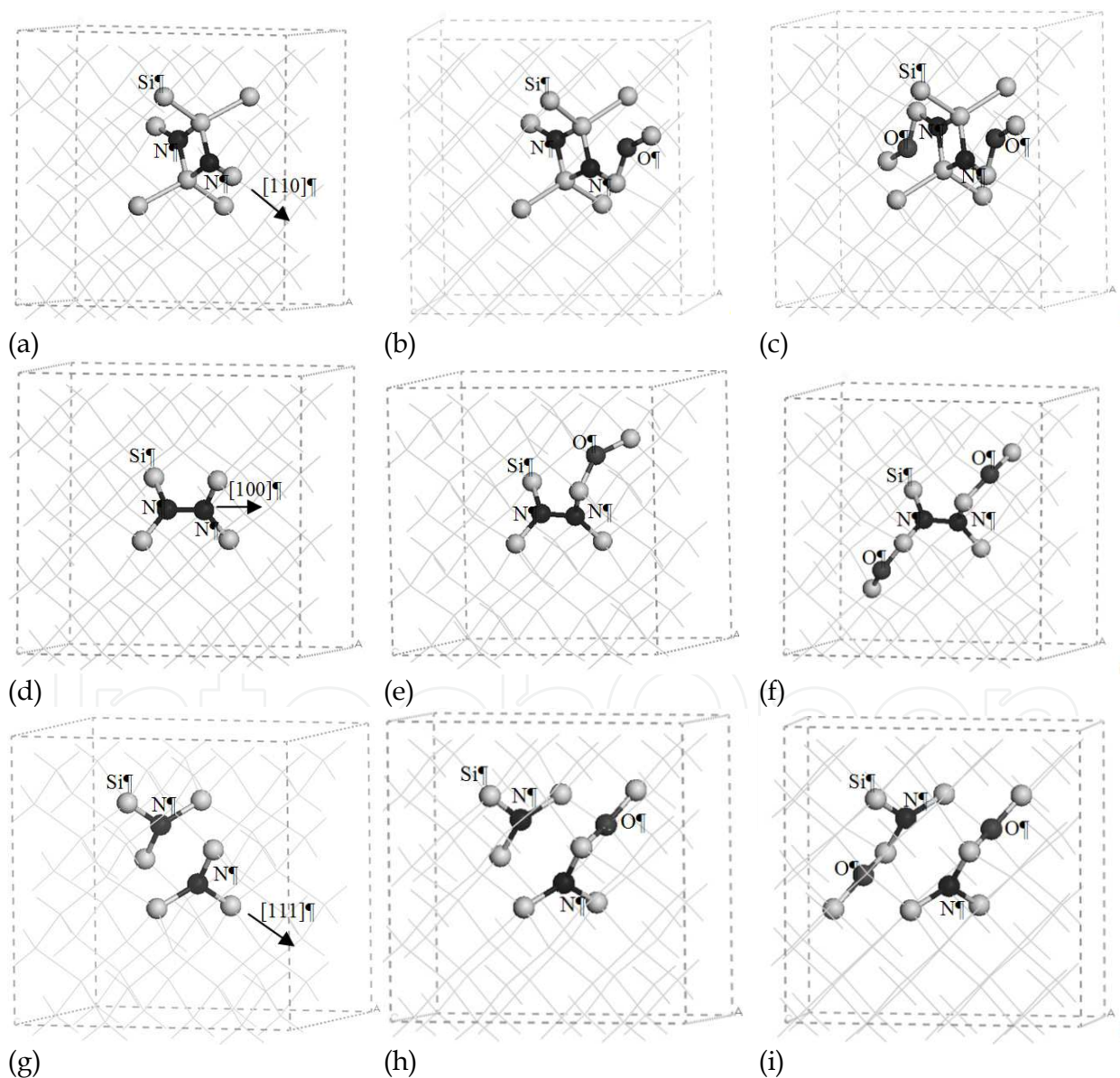


Fig. 10. N-Pair defects atomic structure (a, b, c) N_2 (C_{2h}), N_2O , N_2O_2 ; (d, e, f) VN_2 (D_{2d}), VN_2O , VN_2O_2 ; (g, h, i) V_2N_2 (D_{3d}), V_2N_2O , $V_2N_2O_2$.

configuration, as proposed by Jones et al. (Jones et al., 1994). The four Si-N bonds form a diamond shape lying in (110) plane. The bond centered interstitial configuration for N₂ has been found energetically favorable based on ion channeling, infrared absorption, and theoretical calculations (Jones et al., 1994).

As shown in Fig. 10 (d), neutral VN₂ complex is formed by inserting an N-N pair at a vacancy site in the center of a tetrahedron (Stein, 1986). The central bond of the N-N pair is aligned along <100> whereas the four N-Si bonds point to the summits of the tetrahedron, and lie in two perpendicular {110} planes which makes the symmetry group of VN₂ of D_{2d} type, Fig. 11.

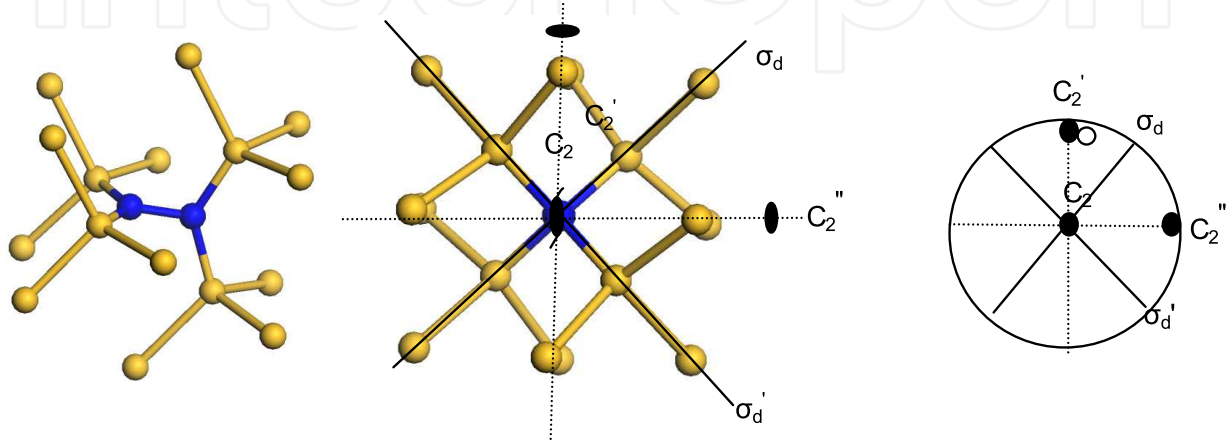


Fig. 11. VN₂ molecule Structure in Si, symmetry point group D_{2d} and stereographic projection.

The V₂N₂ complex is created by inserting two N atoms in the vacancy sites of a relaxed divacancy, see Fig. 10 (g). The divacancy six silicon dangling bonds are fully reconstructed. V₂N₂ has a D_{3d} symmetry (Fig. 13) similar to the ideal divacancy with “breathing” bonding (Coomer et al., 1999), see Fig. 12.

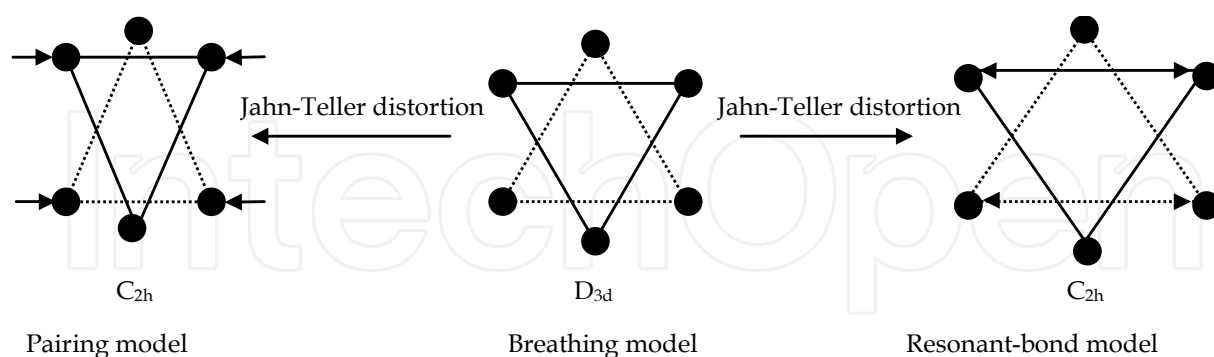


Fig. 12. Si divacancy Jahn Teller distortion (Coomer et al., 1999; Watkins & Corbett, 1965).

The N-O complexes object of this study, result from the coupling of a N-N core defect product of chemical reactions R1 thru R5, with an oxygen interstitial (O_i) or an oxygen dimer (O₂) as shown in the chemical reactions R6 thru R11:





The atomic structures of N_2O , VN_2O and V_2N_2O complexes are obtained by adding one O_i atom on the dilated Si-Si bond neighboring the N-N center as shown in Fig. 10 (b), (e), (h). Indeed, previous investigations on oxygen interstitial in silicon (Umerski, 1993) showed that oxygen bridges dilated Si bonds preferentially along $\langle 111 \rangle$ directions. Likewise, the N_2O_2 , VN_2O_2 and $V_2N_2O_2$ are built by inserting two O_i atoms on Si-Si dilated bonds neighboring the N-pair, Fig. 10 (c), (f), (i).

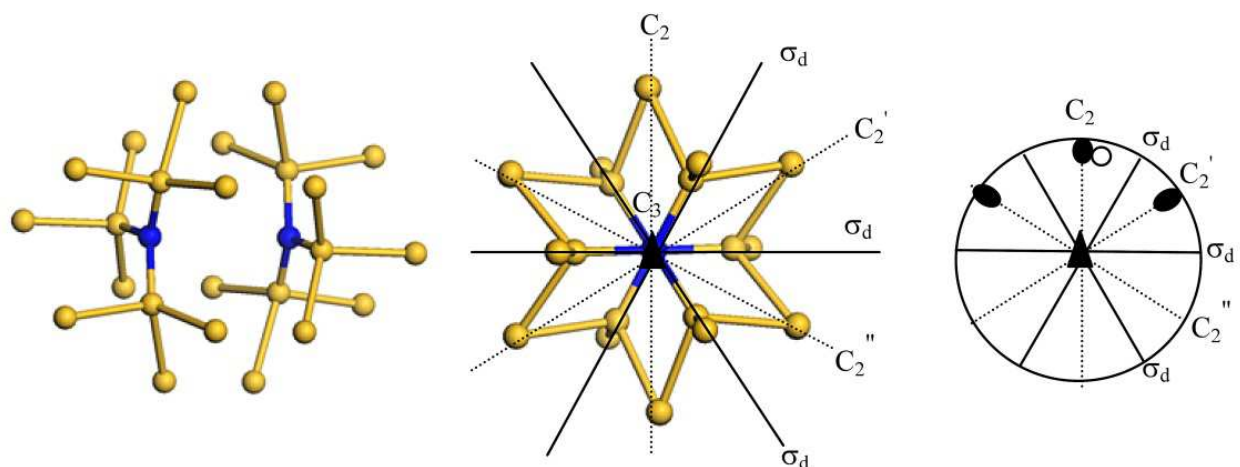


Fig. 13. V_2N_2 molecule Structure in Si, symmetry point group D_{3d} and stereographic projection.

5.2.2 Equilibrium structure and energy of formation

To cut down the computation time, the defected supercells were first relaxed using a valence force field method with COMPASS potential and then DFT Fastructure program (Fastructure). This allowed a fast cleanup and optimization of the guessed atomic structure. Fastructure determines the ground state energies and forces within the Harris functional (Harris, 1985), an approximate scheme of the DFT scheme of Kohn and Sham (Kohn & Sham, 1965). For this scheme, the exchange-correlation terms are calculated using the Vosko, Wilk, Nusair (VWN) parameterization (Vosko et al., 1980) and the radial cutoff was set at 10\AA . The optimizations of the resulting structures were then performed using DFT program DMol³. DMol³ utilizes a basis set of numeric atomic functions that are exact solutions to the Kohn-Sham equations for the atoms (Delley, 1995). For the present study, a doubled numerical basis set with d-polarization functions, termed DND basis set, was used as it ensures an accurate description of the bonding environment. This basis set is well parameterized for nitrogen, oxygen, and Si atoms that are bonded to neighbors by sp^3

hybrid electron orbital that protrude in a tetrahedral shape. Perdew-Wang functional was used for the exchange correlation terms. To accelerate the convergence of the self-consistent-field (SCF) procedures we use the direct inversion of the iterative subspace method (DIIS) (Pulay, 1980). Integration over the Brillouin-zone and over all occupied orbital is done with the tetrahedron method (Blöchl, 1994) and equispaced Fourier meshes similar to the ones proposed by Monkhorst and Pack (Monkhorst, 1976). Eight k-points and 24 tetrahedra were used to sample the Brillouin zone. The atomic positions were optimized using the Broyden-Fletcher-Goldfarb-Shanno (BFGS) quasi-Newton optimization algorithm.

For the general chemical reaction $X_A + X_B \rightarrow X_C$, the formation energy of the product X_C is defined as (Nichols, 1989):

$$E_f(X_C) \equiv E(X_C) + E_{bulk} - E(X_A) - E(X_B) \quad (31)$$

Where $E_f(X_C)$ denotes the formation energy of the complex, $E(X_i)$ the total energy of the system containing a reactant or a product, and E_{bulk} is the total energy of pure bulk Si supercell.

All reactants and products involved in reactions R1 through R11, including the Si vacancy (V) and the Si divacancy (V_2) which are important for our study, have been optimized with the same level of theory and accuracy. As reference, our calculations suggest a formation energy of 3.89 eV for the Si vacancy and 5.80 eV for the divacancy in good agreement with previously published values (3.31-3.98 eV) for the vacancy (Hull, 1999; Puska et al., 1998) and 4.4-5.7 eV for the divacancy (Hull, 1999; Pesola, 2000). During relaxation, the neutral Si divacancy (V_2) are usually subject to Jahn-Teller (JT) distortion which lower the symmetry of the defect from trigonal D_{3d} to monoclinic C_{2h} resulting in the 'pairing' or 'resonant-bond' structure (Coomer, 1999; Pesola, 2000; Watkins, 1965), see Fig. 12. Our calculations exhibit a 'large pairing' JT distortion for the relaxed V_2 rather than a 'resonant bonding' distortion, in line with positron annihilation spectroscopy measurements (Nagai, 2003). The reconstructed bonds of the divacancy form two co-planar isosceles triangles, the length of the two congruent sides of the triangles is about 4.44 Å, and the base is about 3.54 Å long.

5.2.3 Computation of vibrational spectra

The absorption spectrum for each optimized atomic structure was calculated using the eigenvalue method (Dean & Martin, 1960) implemented in DMol³ package. The eigenvalue method is sensitive to the accuracy of the calculated electronic structure; therefore vibrational analysis can be meaningful only when all atomic forces are zero. This is attainable only when the geometry is optimized at the same level of theory and with the same basis set used to generate the Hessian.

Since, there is at present no method for calculating the intensities of IR active LVMs for periodic boundary environment because the Hessian in internal coordinates can not be evaluated in that case, the LVM intensities were computed using the MNDO method and the Austin Model 1 (AM1) Hamiltonian (Dewar et al., 1985). MNDO works only on molecular systems therefore a crystal macro-molecule (CMM) has been extracted from the Dmol³ relaxed supercell. Each CMM contains the N-N core defect in its center surrounded by 76 silicon, and 74 hydrogen atoms which saturate the dangling bonds at the surface. The N-N core is totally surrounded by as much Si atoms as possible to properly simulate the host crystal. Given the fact that the CMM is relatively small, special care was taken to ensure that the symmetry is not broken for the defect and neighboring silicon atoms.

MNDO-AM1 method considers only valence electrons in the calculation of the electronic states, treating the inner-shell electrons together with the nucleus as a core. The electron-electron, core-core, and core-electron interactions are obtained empirically. We used a restricted closed-shell wavefunctions, which constrain all molecular orbitals to be either doubly occupied or empty.

Within DMol³ and MNDO-AM1 the LVMs are determined from the Hessian matrix using the Harmonic Oscillator Approximation. This approach is known to adequately describe the vibrational behavior of molecules and crystals at low temperature, where only the lowest vibrational levels are populated and the displacements from equilibrium are small. Usually, the harmonic vibrational frequencies produced by ab-initio calculations are larger than the experimentally fundamental lines by 5 to 10%. Both methods neglect the effect of anharmonicity, which is insignificant at the ground state.

The force constant for each pair of bonded atoms are obtained by diagonalization of the mass-weighted Hessian matrix element, defined as:

$$H_{i,j}^m = \frac{1}{\sqrt{m_i m_j}} \frac{\delta^2 E}{\delta x_i \delta x_j} \quad (32)$$

Only change in the dipole moment induces measurable IR transitions. For bonds which have a weak dipole moment the polarizability is usually high and the vibrational states of the bond are Raman active (RA). These two kinds of activities are not always mutually exclusive as for non-centrosymmetric molecules (or unit cells), some vibrations can be both Raman and infrared active.

The IR absorption intensity I_i and effective charge e_i of the i^{th} normal mode are evaluated from the dipole moment derivatives with respect to the vibrational coordinates q_i such that I_i is proportional to e_i^2 (Leigh & Szigetti, 1967; Whalley, 1972):

$$I_i = \frac{N_0 \pi}{3c^2 (4\pi\epsilon_0)} e_i^2 \quad (33)$$

$$e_i = \left[\left(\frac{\partial p_x}{\partial q_i} \right)^2 + \left(\frac{\partial p_y}{\partial q_i} \right)^2 + \left(\frac{\partial p_z}{\partial q_i} \right)^2 \right]^{1/2} \quad (34)$$

where N_0 is the Avogadro number, c the speed of light, ϵ_0 dielectric constant in vacuum and p the electrical dipole moment:

$$p = \sum_i e_i q_i \quad (35)$$

The dipole moment derivatives are accurately calculated from the energy gradients $\frac{\partial E}{\partial q_i}$

(Galabov & Dudev, 1996)

$$\frac{\partial p}{\partial q_i} = \frac{\partial}{\partial f} \left(\frac{\partial E}{\partial q_i} \right) \quad \text{where} \quad \frac{\partial E}{\partial q_i} = \left(\frac{\partial}{\partial q_i} \right) \langle \Psi | H - pf | \Psi \rangle \quad (36)$$

Where f is the applied electric field, ψ the wavefunction and H the Hamiltonian. The calculated IR active modes were compared to the measured low temperature ($T < 15K$) FTIR absorption bands since the vibrational spectra are calculated from the ground state specifically from the minimum energy at 0 K corrected by the zero point energy.

5.3 Results and discussion

5.3.1 Formation energy of N_2 , VN_2 , and V_2N_2 complexes

The equilibrium geometries for N-pair defects are summarized in terms of bond length, bond angle in Table 6. The formation energies are summarized in Table 7. We found that the formation energy for N_2 (reaction R1) is about -3.95 eV at the ground state showing that N_2 is a very stable complex. Being highly exothermic, we believe that chemical reaction R1 occurs at earliest stages of point defect clustering, mainly at high temperature close to the melting point (1423°C) because of the high mobility of N_i . N_i has a low diffusion barrier of 0.4 eV (Schultz & Nelson, 2001).

| | N-N (Å) | Si-N (Å) | Si-Si (Å) (1 st neighbor) | \angle Si-N-Si | \angle N-Si-N | \angle Si-N-N |
|----------|---------|-----------|---|------------------|-----------------|-----------------|
| N_2 | 2.45 | 1.73,1.76 | 2.32, 2.40 | 90.8 | 89.2 | - |
| VN_2 | 1.43 | 1.80 | 2.33, 2.42 | 131.4 | - | 114.4 |
| V_2N_2 | 3.55 | 1.82 | 2.38, 2.35 | 118 | - | - |

Table 6. N-pair relaxed geometry parameters from DFT-DMol³ calculations.

| E_f (eV) | N_2 | VN_2 | V_2N_2 | N_2O | N_2O_2 | VN_2O | VN_2O_2 | V_2N_2O | $V_2N_2O_2$ |
|---|-------|-------------------------------|--------------------------------|--------|----------|---------|-----------|-----------|-------------|
| DFT DMol ³ (this work) | -3.95 | -0.21 (R2) -1.8 (R3) | -4.62 (R4) -4.42 (R5) | -0.96 | -1.4 | -0.15 | +0.51 | -0.70 | -0.95 |
| Harris functional and VWN (Karoui et al. 2003; Sahtout Karoui,2004) | -4.1 | +2.0 | -5.2 -1.0 | -0.78 | -1.52 | +0.08 | +0.33 | -0.62 | -1.31 |
| (Sawada et al., 2000) | -4.3 | -1.4 | -4.55 -5.69 | | | | | | |
| (Kagashima et al., 2000) | -3.86 | +0.33 | -4.07 -3.61 | | | | | | |
| (Goss et al., 2003) | -3.67 | -1.3 | -3.7 -3.4 | | | | | | |
| (Kagashima et al., 2003) | | | | | | | | | -0.95 |

Table 7. Formation energy of N-N and N-O defects from DFT-DMol³ Calculations.

The formation energy of VN_2 complex is about - 0.21 eV when formed from N_i and N_s (reaction R2) and is about -1.8 eV thus more stable, when formed from the coupling of N_2 with a Si vacancy (reaction R3). Reaction R2 occurs mainly when N_i and N_s coexist i.e. near melting temperature of Si. Nevertheless, the small energy gain suggests that VN_2 would easily dissociate at such high temperature. The formation of VN_2 complexes is more likely to happen through reaction R3 during the interstitial-substitutional diffusion process of N_2 around the void formation temperature. This infers that VN_2 should intermittently slip back to N_2 via reaction $\text{VN}_2 + I \rightarrow \text{N}_2$ and back to VN_2 through reaction $\text{N}_2 + V \rightarrow \text{VN}_2$ as suggested in (von Ammon et al., 2001). Though, VN_2 is a metastable complex, it is also foreseen as an active complex during crystal growth as it contributes to the formation of very stable grown-in N-related microdefects such as V_2N_2 (reaction R4 and R5). Indeed, our calculations show that both reactions forming V_2N_2 complexes are highly exothermic. The energy gain is about -4.62 eV for R4 and -4.42 eV for R5 revealing the high stability of V_2N_2 complexes independently of the chemical reaction pathway. The formation of V_2N_2 from the coupling of VN_2 with a vacancy is favored over the coupling of N_2 with a divacancy because V_2 cannot form at high temperature (crystal growth temperature). However, reaction R5 might occur during crystal cooling at temperatures lower than 300°C, the survival temperature range of V_2 . Indeed, V_2 is known to be immobile and stable at room temperature and to anneal out around 200-300°C. The calculated formation energy for N_2 , VN_2 (R3) and V_2N_2 agree with previous work (Sawada et al., 2000; Kagashima et al., 2000; Goss et al., 2003).

5.3.2 Vibrational spectra of N_2 , VN_2 , and V_2N_2 complexes

As shown in Table 8, N_2 interstitial display four vibrational modes among them two are IR active asymmetric stretching, 779 cm^{-1} and 986 cm^{-1} , and two Raman active symmetric stretching (dipole-forbidden), 743 cm^{-1} and 1084 cm^{-1} . Since, the symmetry group of N_2 is C_{2h} , it has normal modes belonging to the irreducible representations A_g , B_g , A_u , and B_u ; A_g and B_g being Raman active, A_u and B_u IR active. The selection rule for absorption in the IR spectrum is that the vibration must have the same symmetry as a p -orbital. Choosing z as the principal axis of symmetry (axis C_2 for C_{2h}), 779 cm^{-1} line transforms as B_u by the symmetry operations of the group, which has the same symmetry as p_x and p_y orbitals. Vibrational mode 986 cm^{-1} transforms as A_u which has the same symmetry as the p_z orbital. The two IR active modes relate to nitrogen. In these modes, the two N atoms are dynamically coupled and move in the same direction, along [001] and [110] respectively, see Fig. 14 (a), (b). These two lines match measured FTIR frequencies 771 cm^{-1} and 967 cm^{-1} . The absorption intensity ratio $\alpha(779)/\alpha(986)$ between the two IR modes as given by MNDO-AM1, is about 0.78. Lines 1084 and 743 cm^{-1} transform as A_g and B_g respectively and are Raman active with the same symmetry as s - and d -orbitals. For these modes, the N atoms move in opposite directions along [110] and [001], respectively. Our calculated LVMs for N_2 agree with reported values by Goss et al (Goss et al., 2003).

VN_2 complex has two IR active LVMs, 585 cm^{-1} and 781 cm^{-1} , and one Raman active line 997 cm^{-1} , see Table 9. The symmetry group of VN_2 is D_{2d} which has normal modes belonging to the irreducible representations A_1 , A_2 , B_1 , B_2 , and E . A_1 and B_1 are Raman active; B_2 and E are IR and Raman active with E representation doubly degenerate. The 585 cm^{-1} mode transforms as B_2 and involves an in-phase asymmetric stretching of the two N atoms along [001]. The 781 cm^{-1} absorption band is doubly degenerate and thus belongs to the E

| Symmetry | Vibrating atoms | Frequencies (cm ⁻¹) | | Intensity (km/mol) ¹ | Effective Charge(e) ¹ | Activity |
|-----------------------------------|-----------------------|---------------------------------|--------------------------------|---------------------------------|----------------------------------|----------|
| | | Calculated | Measured (T<15K) | | | |
| N₂ | | | | | | |
| (C _{2h}) B _g | N-N | 743 | | 0 | 0 | RA |
| B _u | N-N | 779 | | 335 | 0.59 | IR |
| A _u | N-N | 986 | | 542 | 0.75 | IR |
| A _g | N-N | 1084 | | 0 | 0 | RA |
| N₂O | | | | | | |
| | O(v ₁) | 666 | | 33 | 0.18 | IR |
| | N-N | 750 | 771, 967 | 19 | 0.14 | IR |
| | N-N | 814 | (551,653,782,790)* | 316 | 0.59 | IR |
| | N-N+ | 1003 | | 975 | 1.02 | IR |
| | O(v ₃) | | | | | |
| | N-N+ | 1029 | | 289 | 0.55 | IR |
| | O(v ₃) | | | | | |
| | N-N | 1137 | | ~0 | ~0 | RA |
| N₂O₂ | | | | | | |
| | O-O(v ₁) | 658 | | 105 | 0.32 | IR |
| | O-O(v ₁) | 665 | 806,815,1000, 1021, 1031, 739* | 0 | 0 | RA |
| | N-N | 780 | | 0 | 0 | RA |
| | N-N | 825 | | 409 | 0.66 | IR |
| | N-N | 945 | | 1083 | 1.07 | IR |
| | O-O (v ₃) | 1016 | | 0 | 0 | RA |
| | O-O(v ₃) | 1019 | | 482 | 0.71 | IR |
| | N-N | 1027 | | 0 | 0 | RA |

¹ As given by semi-empirical MNDO-AM1 quantum mechanics calculations on a macro-molecule.

Table 8. Vibrational spectra for N₂, N₂O and N₂O₂ from DFT-DMol³ Calculations.

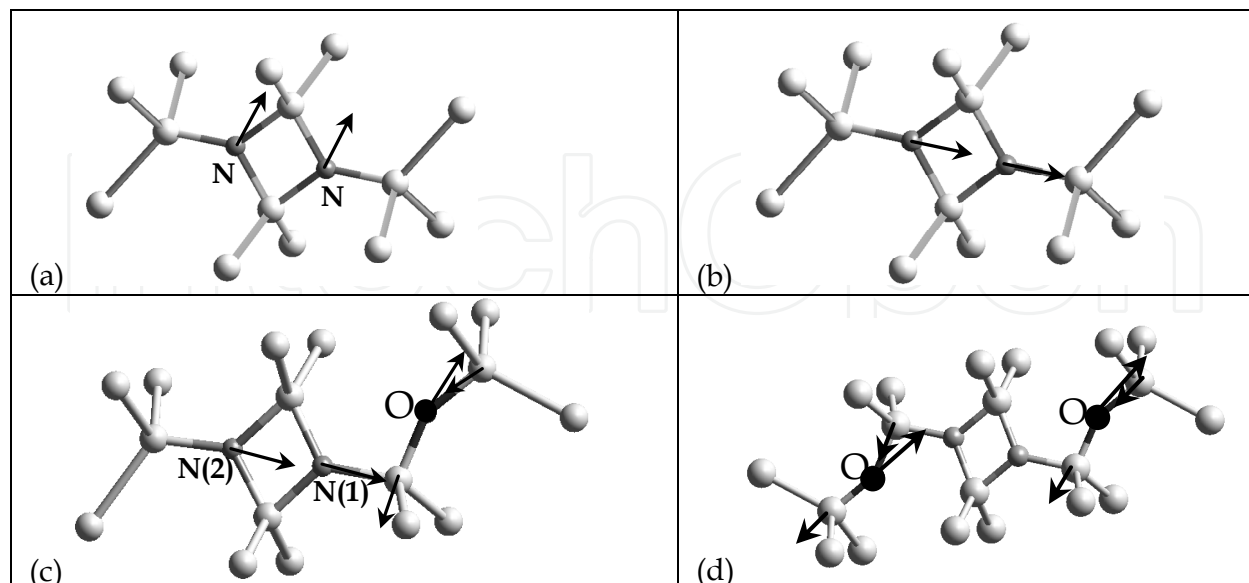


Fig. 14. (a) N₂ 779 cm⁻¹ N-N asymmetric stretching along [001]; (b) N₂ 986 cm⁻¹ N-N asymmetric stretching along [110]; (c) N₂O: 1003 cm⁻¹ N-N + O (v₃) asymmetric stretching; (d) N₂O₂ 1019 cm⁻¹ O (v₃) asymmetric stretching.

| | Symmetry | Vibrating atoms | Frequency (cm ⁻¹) | | Intensity (km/mol) | Effective Charge (e) | Activity |
|---------------------------------------|----------------|----------------------|-------------------------------|-------------------------------------|--------------------|----------------------|----------|
| | | | calculated | Measured (T<15K) | | | |
| VN ₂ (D _{2d}) | B ₂ | N-N | 585 | | 107 | 0.33 | IR |
| | E | N(1) ¹ | 781 | | 183 | 0.43 | IR |
| | | N(2) ¹ | 781 | | 183 | 0.43 | IR |
| | A ₁ | N-N | 997 | | 0 | 0 | RA |
| VN ₂ O | | N-N | 578 | 771, 967 (551, 653, 782, 790)* | 124 | 0.36 | IR |
| | | O(ν ₁) | 642 | | ~ 0 | - | IR |
| | | N(1) | 797 | | 141 | 0.38 | IR |
| | | N(2) | 835 | | 141 | 0.38 | IR |
| | | N-N | 985 | | 0 | 0 | RA |
| | | O(ν ₃) | 1049 | | 320 | 0.57 | IR |
| | | | | | | | |
| VN ₂ O ₂ | | N-N | 567 | | 121 | 0.35 | IR |
| | | O-O(ν ₁) | 644 | 806, 815, 1000, 1021, 1031, 739* | ~ 0 | - | IR RA |
| | | N-N | 819 | | 208 | 0.44 | IR |
| | | N-N | 828 | | 208 | 0.44 | IR |
| | | N-N | 976 | | 0 | 0 | RA |
| | | O-O(ν ₃) | 1103 | | 302 | 0.55 | IR |
| | | O-O(ν ₃) | 1113 | | 0 | 0 | RA |

¹ N(1) and N(2) are respectively, the inner and outer nitrogen atom in the N-N-Si-O-Si branch.

Table 9. Vibrational spectra for VN₂, VN₂O and VN₂O₂ defects using DFT-DMol³ Calculations.

representation. For this mode, the N atoms are dynamically decoupled moving in opposite direction along [110] and [$\bar{1}$ 10] respectively. 781 cm⁻¹ vibrational mode is close to measured 782 and 790 cm⁻¹ lines due to unknown defects (Goss et al., 2003) which probably relate from our calculations to VN₂ defects. VN₂ IR active lines have equivalent strength. The Raman active mode 997 cm⁻¹ transforms as A₁ and involves an in-phase symmetric stretching of the nitrogen atoms along the principal axis [001]. The calculated frequencies for VN₂ as well as their spectroscopy activity are in accordance with reported values for the N_i-N_s complex (Goss et al., 2003). The 585 cm⁻¹ line matches measured 551 cm⁻¹ band detected in N-implanted and laser annealed FZ Si wafer which was attributed to N-substitutional (Stein, 1985). We believe that 551 cm⁻¹ line is due to a localized vibration mode of VN₂ defect in N-implanted FZ Si crystals where vacancies are in excess.

V₂N₂ complex has three degenerate LVMs, each one IR and RA active, 615 cm⁻¹, 625 and 637 cm⁻¹, Table 10. The 615 cm⁻¹ line is weak and involves an in-phase asymmetric (IR active mode) and a symmetric stretching (RA active mode) of the N atoms along the pair axis in the [111] direction with a small deviation along [100]. In this mode, the N atoms are dynamically coupled and the Si-N bonds stretch in a same way. The 625 cm⁻¹ and 637 cm⁻¹ modes involve each one a ν₃ type in-phase asymmetric (IR active mode) and a symmetric (RA active mode) vibration of the N atoms in the plane perpendicular to the pair axis. V₂N₂ structure has a D_{3d} symmetry which has normal modes belonging to A_{1g}, E_g, A_{2u}, E_u irreducible representation. A_{1g} and E_g are Raman active, and A_{2u}, E_u are IR active. E-type

| | Symmetry | Vibrating atoms | Frequencies (cm ⁻¹) | | Intensity (km/mol) | Effective Charge (e) | Activity |
|--|-----------------|-----------------|---------------------------------|-----------------------|--------------------|----------------------|----------|
| | | | Calculated | Measured (T<15K) | | | |
| V ₂ N ₂ | D _{3d} | | | | | | |
| | E _u | N-N | 615 | 771, 967 | 19 | 0.04 | IR, RA |
| | E _g | | | | | | |
| | E _u | N-N | 625 | (551, 653, 782, 790)* | 115 | 0.24 | IR, RA |
| | E _g | | | | | | |
| | E _u | N-N | 637 | | 236 | 0.49 | IR, RA |
| E _g | | | | | | | |
| V ₂ N ₂ O | | O(ν_1) | 651 | | 43 | 0.11 | IR, RA |
| | | N(1) | 696 | | 168 | 0.41 | R |
| | | N(1) | 709 | | 172 | 0.42 | IR |
| | | N(2) | 731 | 806, 815, 1000, 1021, | 201 | 0.51 | IR |
| | | N(2) | 819 | 1031, 739* | 201 | 0.51 | IR |
| | | O(ν_3) | 1068 | | 389 | 0.63 | IR |
| V ₂ N ₂ O ₂ | | O-O(ν_1) | 649 | | 0 | 0 | RA |
| | | N-N | 729 | | 358 | 0.6 | IR RA |
| | | N-N | 810 | | 210 | 0.46 | IR,RA |
| | | O-O(ν_3) | 1061 | | 702 | 0.84 | IR,RA |

Table 10. Vibrational spectra for V₂N₂, V₂N₂O and V₂N₂O₂ defects from DFT-DMol³ Calculations.

modes are double degenerate. We found that V₂N₂ relaxes in D_{3d} structure, each LVM pair pertains to the (E_u, E_g) irreducible representations. This in accordance with Cunha et al. (Cunha, 1993) whose work also reported that a substitutional N₂ having a D_{3d} structure preserve the D_{3d} symmetry during relaxation, while Goss et al. calculations (Goss et al., 2003) showed that a starting C_{3v} geometry relaxed in D_{3d} structure. FTIR measured 653 cm⁻¹ line detected in N-implanted FZ Si is close to calculated IR modes for V₂N₂ defect, which show that this line is generated by localized vibrational modes of N substitutional as stated by Stein (Stein, 1985). The calculated absorption spectra for N₂, VN₂ and V₂N₂ are shown in Fig. 15. We can easily see that N₂ complex bears the highest absorption intensity and that measured 771 and 967 cm⁻¹ lines are IR signature for that defect.

5.3.3 Formation energy of N₂O_n, VN₂O_n, V₂N₂O_n complexes (n=1, 2)

The equilibrium geometries for N-O defects are summarized in terms of bond length, bond angle in Table 11. When N₂ captures an O atom, the energy gain is about 0.96 eV for N₂O. When O_{2i} is trapped by the N-pair (N₂O₂), the energy gain is about 1.4 eV. Likewise, the energy gain is about 0.70 eV and 0.95 eV for V₂N₂O and V₂N₂O₂, respectively. In contrary, the chemical reaction forming VN₂O (R8) is slightly exothermic (E_f = - 0.15 eV), and when capturing an oxygen dimer (R9), the formation energy becomes positive (0.51 eV) meaning that the so-formed VN₂O₂ is unstable. Although, the chemical reactions which form N₂O_n and V₂N₂O_n (n=1,2) are energetically favorable, the limited energy gain render these complexes unstable at elevated temperature. Upon heating, the oxygen atoms would break free and easily diffuse in the matrix, leaving the N-pair intact. Indeed, FTIR measurements have shown a reversible formation and dissociation mechanism between N-N and N-O complexes upon successive heating and cooling (Wagner et al., 1988; Qi et al., 1992).

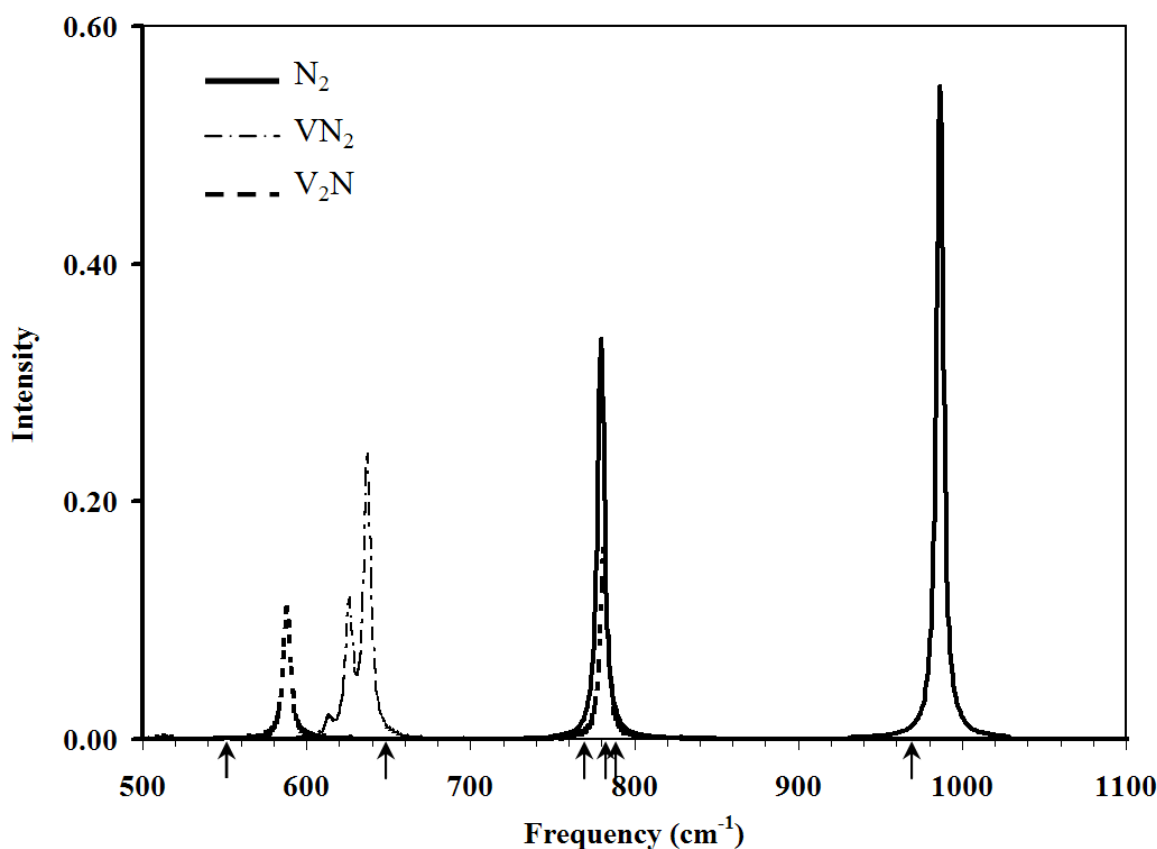


Fig. 15. Vibrational spectra of N_2 , VN_2 and V_2N_2 complexes from DFT-DMol³ Calculations. The arrows shows the FTIR measured frequencies.

| | N-N (Å) | Si-N (Å) | Si-O (Å) | Si-Si (Å) (1 st neighbor) | ∠Si-O-Si |
|-------------|---------|---|----------------|---|----------|
| N_2O | 2.43 | 1.70 (O), 1.72 1.74 (sides of the diamond) 1.68 | 1.64 (N), 1.66 | 2.30 (O) 2.31-2.38 2.29 | 136 |
| N_2O_2 | 2.38 | 1.73 (sides of the diamond structure) | 1.64 (N), 1.65 | | 136.6 |
| VN_2O | 1.44 | 1.77 (O), 1.80 | 1.62 (N), 1.64 | 2.29-2.42 (O) 2.33-2.44 | 141.5 |
| VN_2O_2 | 1.45 | 1.77 (O), 1.80 | 1.61 (N), 1.63 | 2.29-2.42 2.33-2.41 (O) | 147 |
| V_2N_2O | 3.62 | 1.77 (O), 1.82 | 1.61 (N), 1.65 | 2.35-2.40 | 143.6 |
| $V_2N_2O_2$ | 3.72 | 1.77 (O), 1.79, 1.82 | 1.62 (N), 1.65 | 2.34-2.41 | 143.5 |

Table 11. N-O complexes relaxed geometry parameters from DFT-DMol³ calculations. (O) means Si-N bond length in the N-Si-O-Si branch; (N) means Si-O bond length in the N-Si-O-Si branch.

5.3.4 Vibrational spectra of N_2O and N_2O_2 complexes (n=1,2)

Calculated vibrational spectra for N_2O displays five IR active LVMs 666, 750, 814, 1003, and 1029 cm^{-1} and one dipole forbidden transitions at 1137 cm^{-1} , see Table 8. These lines shift to 658, 665, 825, 945 and 1019 cm^{-1} for N_2O_2 . The 779 cm^{-1} mode of N_2 shifts to 814 cm^{-1} when

capturing one O atom (N_2O) and to 825 cm^{-1} when capturing an oxygen dimer (N_2O_2). This blue shift can be explained by the shortening of the N-Si bonds as a result of the insertion of the O atom(s) in the vicinity which causes the N-Si bond stretching force constant to increase so the frequency. As for N_2 , the 814 cm^{-1} and the 825 cm^{-1} modes involve N-N asymmetric stretching in the $[1\bar{1}0]$ direction, with the highest absorption strength on the nitrogen atom neighboring the O atom in the N_2O complex. These two modes are close to the measured 806 cm^{-1} and 815 cm^{-1} FTIR frequencies, ascribed respectively to NNO and NNO₂ defects (Jones et al., 1994). The 750 cm^{-1} mode is a symmetric stretching of the N atoms in $[110]$. This mode has a small strength because of the imbalanced mass due to the O atom in the vicinity of one N atom. The 1003 cm^{-1} mode (N_2O) combines a Si-O-Si asymmetric stretching of ν_3 type (Fig. 7) and an in-phase N-N asymmetric stretching along $[110]$ analog to the N_2 986 cm^{-1} mode, a blue shift of 17 cm^{-1} , see Fig. 14 (c). This frequency matches the measured 1000 cm^{-1} absorption band. N_2 986 cm^{-1} wavenumber shifts down to 945 cm^{-1} when an oxygen dimer interacts with N_2 producing N_2O_2 . As for N_2 , this mode involves an N-N asymmetric stretching along $[110]$. The 945 and 1003 cm^{-1} frequencies have almost identical strength and bear the highest absorption intensity. N_2O 1029 cm^{-1} mode involves an N-N asymmetric stretching combined with a vibration of ν_3 type on the O atom. N_2O_2 1019 cm^{-1} mode is of ν_3 type and involves only the O atoms, see Fig. 14 (d).

Several low frequency local vibrational modes appeared in our calculations. These modes are of ν_1 type (Fig. 7) and are entirely due to Si-O stretch. The 666 cm^{-1} (N_2O) and 658 cm^{-1} (N_2O_2) vibrational modes are IR active, 665 cm^{-1} (N_2O_2) is Raman active. Our results show that calculated 814 , 1003 , 1029 cm^{-1} frequencies for N_2O fit (within a margin of less than 1%) the measured 806 , 815 , 1000 , and 1031 cm^{-1} (low temperature) FTIR lines for N-O complexes. Alike, N_2O_2 1019 cm^{-1} mode matches the 1021 cm^{-1} FTIR line. Measured 1021 cm^{-1} is an IR signature for N_2O_2 and 1031 cm^{-1} N_2O in accordance with what has been suggested by Jones et al. (Jones et al., 1994) based on FTIR measurements.

N_2O defect has been previously theoretically investigated (Ewels, 1997; Jones et al., 1994) using AIMPRO method and H-terminated cluster of about the same size as the macromolecule we used in the MNDO-AM1 calculations. Some discrepancies have been found in the AIMPRO calculations especially concerning the O_i vibration modes which were found between the two N modes in contrary to the observation. The O atom has to be displaced close to the neighboring Si atoms in order to fit the experimental lines.

5.3.5 Vibrational spectra of VN_2O_n and $V_2N_2O_n$ complexes ($n = 1, 2$)

VN_2O and VN_2O_2 complexes have several LVMs ranging from 500 to 1100 cm^{-1} , see Table 9. VN_2O has five IR active modes and one Raman active mode. VN_2 585 cm^{-1} line shifts to 578 cm^{-1} for VN_2O and involves as for VN_2 , an in-phase asymmetric stretching of the N atoms along $[100]$. This mode shifts to 567 cm^{-1} for VN_2O_2 .

The degeneracy due to the D_{2d} symmetry of VN_2 is removed by the oxygen atom in the vicinity of the N-N core, which reduces the symmetry of the defect. As a result, VN_2 781 cm^{-1} frequency splits into two IR active lines, 797 cm^{-1} and 835 cm^{-1} for VN_2O defect. The N atoms are now dynamically decoupled. Each mode is of ν_3 type, one for each nitrogen atom, the N atom neighboring the oxygen bearing the highest frequency. 797 cm^{-1} and 835 cm^{-1} lines shift respectively to 819 cm^{-1} and 828 cm^{-1} for VN_2O_2 complex. These normal modes involve the N atoms which are now dynamically coupled and of ν_3 type. The dipole forbidden band 997 cm^{-1} of VN_2 remains IR inactive for VN_2O and VN_2O_2 . This frequency shifts to 985 cm^{-1} for VN_2O

and to 976 cm^{-1} for VN_2O_2 . We observe several additional LVMS involving exclusively the oxygen atom(s). VN_2O 642 cm^{-1} normal mode is of ν_1 type. This mode becomes doubly degenerate for VN_2O_2 and shifts to 644 cm^{-1} which is IR and Raman active. This frequency involves two ν_1 symmetric stretching, one on each O atom. The IR active mode is induced by an in-phase vibration of the two O atoms, while in the RA mode the O atoms move in opposite direction thus does not induce any change in the dipole moment. All ν_1 IR active modes are very weak. VN_2O has a high frequency mode at 1049 cm^{-1} and is caused by a ν_3 type asymmetric stretching of the O atom. This vibrational frequency shifts to 1103 cm^{-1} in VN_2O_2 complex and include an in-phase ν_3 type vibration of the O atoms. VN_2O_2 has a high frequency vibrational mode at 1113 cm^{-1} which is Raman active. For this mode, the O atoms vibrate in opposite directions, each Si-O-Si branch vibration being of ν_3 type. The 1103 and 1113 cm^{-1} frequencies are centered around the well known oxygen interstitial 1107 cm^{-1} line of nitrogen-free CZ silicon; the average shift being $\pm 5\text{ cm}^{-1}$.

$\text{V}_2\text{N}_2\text{O}$ defect has six IR active LVMS, Table 10. The degeneracy observed for V_2N_2 complex is removed and the degenerate levels, split into four IR active modes: 696 , 709 , 731 , and 819 cm^{-1} . The dipole-forbidden transitions for V_2N_2 due to the D_{3d} symmetry are now allowed because of the reduced symmetry. Frequencies 696 cm^{-1} and 709 cm^{-1} involve a vibration of the outer N atom whereas the 731 cm^{-1} and 819 cm^{-1} lines involve a vibration of the inner N atom (neighboring the O atom). These LVMS are of ν_3 type and the N atoms are dynamically decoupled. The frequencies and vibrational intensities of the inner N atom are higher than those of the outer N atom because of the unbalanced mass center. The $\text{V}_2\text{N}_2\text{O}$ complex has a high frequency mode at 1068 cm^{-1} of ν_3 type and involving exclusively the O atom. The 651 cm^{-1} absorption line is a ν_1 symmetric stretching of the O atom and is very weak.

All degenerated LVMS found for V_2N_2 core defect remain degenerated for $\text{V}_2\text{N}_2\text{O}_2$, formed by symmetrically trapping two O atoms. Three are IR and Raman active: 729 cm^{-1} , 810 cm^{-1} , and 1061 cm^{-1} ; and one is Raman active: 649 cm^{-1} . The 729 cm^{-1} and 810 cm^{-1} absorption modes involve respectively, an in-phase symmetric and asymmetric N-N stretching in $[111]$ perpendicular to the N-N center axis, similar to V_2N_2 615 cm^{-1} and 638 cm^{-1} lines. Frequency 649 cm^{-1} and 1061 cm^{-1} are exclusively oxygen atom related. The 649 cm^{-1} mode involves two dynamically coupled ν_1 LVMS, one for each Si-O-Si branch, in opposite phase. The 1061 cm^{-1} is induced by two pairs of coupled ν_3 stretching mode, one for each O atom. One pair is due to a symmetric vibration of the O atoms, therefore does not induce any change in the dipole moment, while the other pair is an asymmetric movement, and is thus IR active. This mode bears the highest strength.

Lines 729 cm^{-1} ($\text{V}_2\text{N}_2\text{O}_2$) or 731 cm^{-1} ($\text{V}_2\text{N}_2\text{O}$) might be assigned to the measured FTIR frequency 739 cm^{-1} observed in samples implanted with both N and O atoms and which was attributed to NNO complex (Berg Rasmussen, 1996). As a matter of fact, ion implantation creates an excess of vacancies that will couple with nitrogen to form the V_2N_2 complexes which will subsequently couple with oxygen. These two modes have equivalent strength. The 810 cm^{-1} ($\text{V}_2\text{N}_2\text{O}_2$) and 819 cm^{-1} ($\text{V}_2\text{N}_2\text{O}$) frequencies fit the FTIR measured 806 cm^{-1} and 815 cm^{-1} absorption lines for N-O defects.

5.3.6 Nucleation of extended defects and nitrogen concentration measurement

In order to comprehend how the N-related defects in N-doped Si shape the nucleation and growth of extended defects, and to accurately assess the nitrogen concentration in N-doped

silicon, it is necessary to compare the properties of each defect obtained from DFT calculations to experimental data. This is done by studying the equilibrium structures, and comparing the calculated vibrational modes with experimental Fourier-transform infrared spectra.

The high stability of N_2 and V_2N_2 complexes should explain the strong change observed in the kinetics of oxygen precipitation and void formation in N-CZ Si as compared to N-free CZ Si. The formation of V_2N_2 complexes lower the vacancy supersaturation during crystal cooling. N_2 might equally reacts with oxygen through reactions R6 and R7 or a silicon vacancy through reaction R3. Reactions R8 and R9 show that VN_2 complexes are less able to react with oxygen but would preferentially react with a Si vacancy (reaction R4) to form the very stable V_2N_2 defects which will in turn act as nucleation sites for oxygen precipitates.

It appears from this study that V_2N_2O and $V_2N_2O_2$ complexes equally compete with N_2O and N_2O_2 as nucleation sites for O precipitation. They are the most stable N-O defects since the capture of O_i or O_2 by N_2 and V_2N_2 are all exothermic reactions, and the N-pair complexes (N_2 and V_2N_2) from which they originate are extremely stable. However, N_2O_n defect should be the dominant defect since our results strongly support the assignment of the FTIR 771 and 967 cm^{-1} (15K) local vibrational modes to N_2' meaning they are experimentally detectable. The process formation of N-O complexes is likely to follow the subsequent chemical pathways: $N_2 \rightarrow VN_2 \rightarrow V_2N_2 \rightarrow V_2N_2O \rightarrow V_2N_2O_2$ and $N_2 \rightarrow N_2O \rightarrow N_2O_2$. Therefore, nitrogen will increase the number of O-precipitates nucleation sites by coupling with vacancies and oxygen atoms, explaining the high density of as-grown oxygen precipitates and the decrease in the vacancy supersaturation observed in N-CZ Si. Consequently, the formation of void will be hindered and their density will decrease compared to N-free CZ Si. These results combined with our previous results obtained from molecular mechanics force field calculations (Karoui et al., 2003; Sahtout Karoui et al., 2004) and experimental measurements (Wright etching, STEM, HRTEM, and Oxygen Precipitates Profiler) (Karoui et al., 2004a, 2004b, 2002) confirm that N_2 and V_2N_2 are much more likely to adsorb O atoms than to trap vacancies thus act as nucleation centers for oxygen precipitation rather than voids. However, N-O complexes might also co-exist in the oxide layer covered walls of the voids in N-doped Si. Indeed, EDS measurements on N-doped CZ Si samples showed that voids are covered with an oxide layer as in the case of undoped crystals (Takahashi et al., 2003).

All studied structures of N-O complex have IR active lines falling around measured 806 and 815 cm^{-1} (15K) lines : 814 cm^{-1} (N_2O), 825 cm^{-1} (N_2O_2), 819 cm^{-1} (V_2N_2O), 810 cm^{-1} ($V_2N_2O_2$), 797 cm^{-1} and 835 cm^{-1} (VN_2O), 819 cm^{-1} and 828 cm^{-1} (VN_2O_2). Therefore, the absorption intensity of lines 806 cm^{-1} and 815 cm^{-1} (15K) have to be taken into account when evaluating nitrogen concentration in N-CZ Si or O-rich N-FZ Si wafers. So, a more accurate calibration relationship for [N] measurement in N-CZ Si or O-rich N-FZ Si would be:

$$[N] = (1.83 \pm 0.24) \times 10^{17} \times [\alpha_{967} + \alpha_{806} + \alpha_{815}] \text{ at/cm}^{-3} \text{ (T<15K)} \quad (37)$$

$$[N] = (1.83 \pm 0.24) \times 10^{17} \times [\alpha_{963} + \alpha_{801} + \alpha_{810}] \text{ at/cm}^{-3} \text{ (at 300K)} \quad (38)$$

This is in agreement the experimental calibration curve proposed by Qi et al. (Qi et al., 1992) based on FTIR measurements. For N-implanted O-rich FZ wafer the absorbance of 653 cm^{-1} line has to be considered in the calibration formula because of the important excess of vacancy created during the implantation process. These absorption bands were found to be due to localized vibration modes of substitutional nitrogen (Stein, 1985) and appear from

this study to actually relate to V_2N_2 complexes, therefore the nitrogen calibration curve for N-implanted FZ-Si wafers would be:

$$[N] = (1.83 \pm 0.24) \times 10^{17} \times [\alpha_{967} + \alpha_{653}] \text{ at/cm}^{-3} \text{ (T<15K)} \quad (39)$$

5.4 Conclusions

To comprehend the effect of nitrogen doping on vacancy aggregation, oxygen precipitation, and nitrogen concentration measurement in silicon, we have theoretically investigated using density functional theory (DMol³) and semi-empirical MNDO-AM1 method, the atomic structure, formation energy, and vibrational spectra of several dominant N-related complexes. The focus was on N-pairs occupying either an interstitial or a substitutional position and the associated N-O complexes consisting of bridging one or two oxygen interstitial atoms on the first Si-Si bond neighboring the N-N center. We found a good correlation between the degree of stability of the defect, the IR active energy levels foreseen by the symmetry of the defect and the calculated and measured IR active modes. We found, in agreement with an earlier theoretical study, that $N_i + N_i \rightarrow N_2$ and $VN_2 + V \rightarrow V_2N_2$ are highly exothermic chemical reaction thus are very stable complexes. Both complexes are believed to chiefly form and coexist during crystal growth. The VN_2 complex is a metastable species playing a central role in the formation of very stable V_2N_2 defects. The N-O complexes formed from N_2 and V_2N_2 defects that is N_2O_n and $V_2N_2O_n$ ($n=1, 2$) are the most stable among studied N-O complexes suggesting that they act as nucleation centers for oxygen precipitation. It is likely that vacancy concentration during crystal growth is affected by the following chemical reaction pathway $N_2 \rightarrow VN_2 \rightarrow V_2N_2 \rightarrow V_2N_2O \rightarrow V_2N_2O$, which decreases the vacancy supersaturation, delaying the onset of vacancy clustering and lessening the void density.

Our results strongly support the assignment of 771 cm^{-1} and 967 cm^{-1} (T<15K) absorption bands to N_2 pairs in split interstitial positions. Our calculations show that 551 cm^{-1} line and 653 cm^{-1} detected in N-implanted FZ Si crystals relates to nitrogen substitutional and are caused by the vibration of VN_2 and V_2N_2 complexes. Unexplained measured 782 and 790 cm^{-1} FTIR lines probably relate to VN_2 defects. Our DFT calculations on N-O complexes show that N_2O and N_2O_2 complexes best match the FTIR absorption bands measured for N-O complexes. N_2O_n , VN_2O_n and $V_2N_2O_n$ ($n = 1, 2$) have IR absorption bands around measured 806 cm^{-1} and 815 cm^{-1} lines and all relate to nitrogen vibrations. We found that FTIR 1021 cm^{-1} absorption band is an IR signature for N_2O_2 and that 1000 cm^{-1} and 1031 cm^{-1} relate to N_2O vibrations. The 739 cm^{-1} line measured in N implanted FZ Si wafers originates from V_2N_2O or $V_2N_2O_2$ vibrations.

The degree of stability and matching infrared vibrational spectra suggest that N_2O_n as well as $V_2N_2O_n$ complexes develop during crystal growth and wafer annealing and that both act as nucleation site for oxygen precipitates. The increase in the number of nucleation sites due to nitrogen-vacancy-oxygen coupling explain the high density of grown-in oxygen precipitates and the delay in void formation observed in N-doped Si crystals.

Since all studied N-O complexes have normal modes falling around 806 cm^{-1} and 815 cm^{-1} (T<15K) measured FTIR lines, these absorption bands have to be considered in the [N] calibration relationship for N-CZ and O-rich N-FZ Si, $[N] = (1.83 \pm 0.24) \times 10^{17} \times [\alpha_{967} + \alpha_{806} + \alpha_{815}] \text{ at/cm}^{-3} \text{ (T<15K)}$. For N-FZ implanted wafer the absorbance of 653 cm^{-1} line which relate to V_2N_2 have to be considered in the calibration formula because of the important excess of vacancy existing in implanted wafers.

6. Acknowledgements

The high performance computing has been carried out through user grants from North Carolina supercomputing center and the high performance computing center at East Carolina State University (U.S.A.). The second author acknowledges partial support by DOD under contract No. W91CRB-10-C-0321.

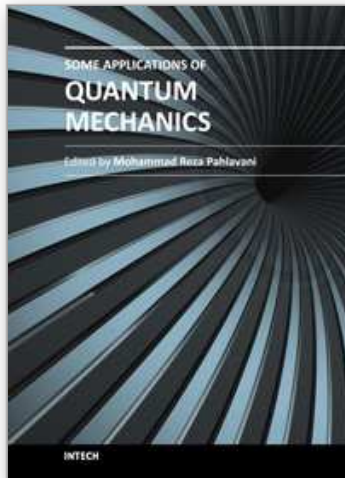
7. References

- Abe, T.; Masui, T.; Harada, H.; & Chikawa, J. (1985). *VLSI science and technology, Proceedings of the Second International Symposium on Very Large Scale Integration Science and Technology*, Electrochemical Society, Pennington, NJ, 1985, pp. 543-550.
- Aihara, K. , Takeno, H.; Hayamizu, Y.; Tamatsuka, M.; & Masui, T. (2000). Enhanced nucleation of oxide precipitates during Czochralski silicon crystal growth with nitrogen doping. *J. Appl. Phys.*, Vol. 88, No. 6, pp. 3705-3707.
- Atkins, Peter; Friedman, Ronald (Ed(s)). (2011). *Molecular Quantum Mechanics*, Oxford University Press Inc, ISBN 978-0-19-954142-3, New York, U.S.A.
- Berg Rasmussen, F.; Öberg, S.; Jones, R.; Ewels, C.; Goss, J.; Miro, J.; & Deák, P. (1996). The nitrogen-pair oxygen defect in silicon. *Mat. Sc. Eng. B*, Vol. 36, pp. 91-95.
- Bernath, Peter F. (Ed(s)). (1995). *Spectra of Atoms and Molecules*, Oxford University Press Inc, ISBN 0-19-507598-6, New York, U.S.A.
- Blöchl, P. E.; Jepsen, O.; & Andersen, O. K. (1994). Improved tetrahedron method for Brillouin-zone integrations. *Phys. Rev. B*, Vol. 49, No. 23, pp. 16223-16233.
- Brower, K.L. (1982). Deep-level nitrogen centers in laser-annealed ion-implanted silicon. *Phys. Rev. B*, Vol. 26, No. 11, pp. 6040-6052.
- Chiou, H-D.; Moody, J.; Sandford, R.; and Shimura, F. (1984). Effects of Oxygen and Nitrogen on slip in Cz Wafers. *VLSI science and technology, Proceedings of the Second International Symposium on Very Large Scale Integration Science and Technology*, Vol. 84-7, pp. 59-65, Cincinnati, Ohio, 1984.
- COMPASS force field potential developed by Accelrys Inc. (USA).
- Coomer, B. J.; Resende, A.; Goss, J. P.; Jones, R.; Oberg, S.; & Briddon, P. R. (1999). The divacancy in silicon and diamond. *Physica B*, Vol. 273-274, pp. 520-523.
- Cunha, C.; Canuto, S.; & Fazio, A. (1993). Role played by N and N-N impurities in type-IV semiconductors, *Phys. Rev. B*, Vol. 48, No. 24, pp. 17806-17810.
- Dean, P.; & Martin, J. L. (1960). A Method for Determining the Frequency Spectra of Disordered Lattices in Two-Dimensions. *Proc. Roy. Soc., A* 259 , No. 1298, pp. 409-418.
- Delley, B. J. (1990).. An all-electron numerical method for solving the local density functional for polyatomic molecules. *J. Chem. Phys.*, Vol. 92, No. 1, pp. 508-517.
- Delley, B. (2000). From molecules to solids with the DMol³ approach. *J. Chem. Phys.*, Vol. 113, Vol. 508, pp. 7756-7764.
- Delley, B. (1995). Modern Density Functional Theory: A Tool for Chemistry. *Theoretical and Computational Chemistry*, Vol.2 ; Elsevier 1995.
- Dewar, M. J. S.; Zoebisch, E. G.; Healy, E. F.; & Stewart, J. J. P. (1985). Development and use of quantum mechanical molecular models. AM1: a new general purpose quantum mechanical molecular model. *J. Am. Chem. Soc.*, 107, pp. 3902-3909.
- Ewels, C. (1997). Density Functional Modelling of Point Defects in Semiconductors, *PhD. Thesis*, University of Sussex, UK.

- Faststructure in Cerius2 package, Accelrys Inc. (USA).
- Fuma, Naoki ; Tashiro, Koichiro; Kakumoto, Katsunori; & Yukio, Takano (1996). Diffused Nitrogen-Related Deep Level in N-Type Silicon. *Jpn. J. Appl. Phys.*, Vol. 35, No. 4A, pp. 1993-1999.
- Galabov, Boris S.; & Dudev, Todor (1996). *Vibrational Spectra and Structure : Vibrational Intensities*, James R. Durig Series Editor, Elsevier, 1996, ISBN 0444814973 & 9780444814975.
- Goss, J. P.; Hahn, I.; Jones, R.; Briddon, P. R ; Öberg, S. (2003). Vibrational modes and electronic properties of nitrogen defects in silicon. *Phys. Rev. B*, Vol.67, 045206-045216.
- Hara, A.; Myabo, T.; & Hirai, L. (1989). Oxygen-nitrogen complexes in silicon formed by annealing in nitrogen. *Appl. Phys. Lett.*, Vol. 54, No. 7, pp. 626-628,
- Harris, Daniel C.; and Bertolucci, Michael D. (Ed(s)). (1989). *Symmetry and Spectroscopy*, Dover publications Inc, ISBN 0-486-66144-X, New York, U.S.A.
- Harris, J. (1985). Simplified method for calculating the energy of weakly interacting fragments. *Phys. Rev. B*, Vol. 31, pp. 1770-1779.
- Hull, Robert (1999). *Properties of Crystalline Silicon*, Institution of Engineering & Technology, 1999, ISBN 978-0-86341-556-2.
- Ikari, A.; Nakai, K.; Tachikawa, Y.; Deal, H.; Hideki, Y.; Ohta, Y.; Masahashi, N.; Hayashi, S.; Hoshino, T.; & Ohashi, W. (1999). Defect Control in Nitrogen Doped Czochralski Silicon Crystals. *Solid State Phenomena*, Vol. 69-70, pp. 161-166.
- Itoh, Y; Nazaki, T.; Masui, T.; Abe, T. (1985). Calibration curve for infrared spectrophotometry of nitrogen in silicon. *Applied Physics Letters*, Vol. 47, No. 5, pp. 488-489.
- Jones, R. ; Oberg, S.; Rasmussen, F. B.; & Nielsen, B. B. (1994). Identification of the dominant nitrogen defect in silicon. *Phys. Rev. Lett.*, Vol. 72, pp. 1882-1885.
- Jones, R.; Ewels, C.; Goss, J.; Miro, J.; Deak, P.; Öberg, S.; & Rasmussen, F. Berg (1994). Theoretical and isotopic infrared absorption investigations of nitrogen-oxygen defects in silicon. *Semicond. Sci. Technol.*, Vol. 9, No. 11, pp. 2145-2148.
- Kageshima, H.; Taguchi, A.; & Wada, K. (2000). Theoretical investigation of nitrogen-doping effect on vacancy aggregation processes in Si. *Applied Physics Letters*, Vol. 76, No. 25, pp. 3718-3720.
- Kageshima, H.; Taguchi, A.; Wada, K. (2003). Formation of stable N-V-O complexes in Si. *Physica B*, Vol. 340-342, pp. 626-629.
- Karoui, A.; Sahtout Karoui, F.; Rozgonyi, G. A.; & Yang, D. J. (2004). Oxygen precipitation in nitrogen doped Czochralski silicon wafers. I. Formation mechanisms of near-surface and bulk defects. *J. Appl. Phys.*, Vol. 96, No. 6, pp. 3255-3263.
- Karoui, A. ; & Rozgonyi, G. A. (2004). Oxygen precipitation in nitrogen doped Czochralski silicon wafers. II. Effects of nitrogen and oxygen coupling. *J. Appl. Phys. II*, Vol. 96, No. 6, pp. 3264-3270.
- Karoui, A.; Sahtout Karoui, F.; Kvit, A.; Rozgonyi, G. A.; & Yang, D. (2002). Role of nitrogen related complexes in the formation of defects in silicon. *Applied Physics Letters*, Vol. 80, No. 12, pp. 2114-2116.
- Karoui, A.; Sahtout Karoui, F.; Rozgonyi, G. A.; Hourai, M.; & Sueoka, K. (2003). Structure, Energetics, and Thermal Stability of Nitrogen-Vacancy-Related Defects in Nitrogen Doped Silicon. *J. of the Electrochem. Soc.*, Vol. 150, No. 12, G771-G777.

- Karoui, F. Sahtout; & Karoui, A. (2010). A density functional theory study of the atomic structure, formation energy, and vibrational properties of nitrogen-vacancy-oxygen defects in silicon. *J. App. Phys.*, Vol. 108, No. 3, pp. p033513- p033525.
- Kohn W. ; & Sham, L. J. (1965). Self-Consistent Equations Including Exchange and Correlation Effects. *Phys. Rev.*, Vol. 140, No. 4A, pp. A1133-A1138.
- Leigh, R.S.; & Szigetti., B. (1967). Absorption by the Vibrations of Uncharged Atoms. *Proc. Roy. Soc.*, Vol. 301, No. 1465, pp. 211-221.
- Monkhorst H. J.; & Pack, J. D. (1976). Special points for Brillouin-zone integrations. *Phys. Rev. B*, 13, pp. 5188-5192.
- Murphy, J.D.; Alpass, C.R.; Giannattasio, A.; Senkader, S.; Falster, R.J.; & Wilshaw, P.R. (2006). Nitrogen in silicon: Transport and mechanical properties. *Nuclear Instruments and Methods in Physics Research*, Vol. 253, No. 1-2, pp. 113-117.
- Nagai, Y. ; Inoue, K.; Tang, Z.; Yonenaga, I.; Chiba, T.; Saito, M.; & Hasegawa, M. (2003). Jahn-Teller distortion of neutral divacancy in Si studied by positron annihilation spectroscopy. *Physica B*, Vols. 340-342, pp. 518-522.
- Nakai, K.; Inoue, Y.; Yokota, H.; Ikari, A.; Takahashi, J.; Tachikawa, A.; Kitahara, K.; Ohta, Y.; Ohashi, W. (2001). Oxygen precipitation in nitrogen-doped Czochralski-grown silicon crystals. *J. Appl. Phys.*, Vol. 89, No. 8, pp. 4301-4309.
- Nichols, C. S.; Van de Walle, C. G.; & Pantelides, S. T. (1989). Mechanisms of dopant impurity diffusion in silicon *Phys. Rev. B*, Vol. 40, No. 8, 5484-5496.
- Pesola, Marko (2000). Electronic Structure Calculations for Vacancies and Oxygen-Related Defects in Semiconductors. *Dissertation Thesis*, Helsinki University of Technology, Finland, 18th of August, 2000, ISBN 951-22-5102-7.
- Pulay, P. (1980). Convergence acceleration of iterative sequences. the case of scf iteration *Chem. Physics Letter*, Vol.73, pp. 393-398.
- Puska, M. J. ; Pöykkö, S.; Pesola, M.; & Nieminen, R. M. (1998). Convergence of supercell calculations for point defects in semiconductors: Vacancy in silicon. *Phys. Rev. B*, Vol. 58, No. 3, pp. 1318-1325.
- Qi, M.W.; Tan, S.S.; Zhu, B.; Cai, P.X.; Gu, W.F.; Xu, X.M.; Shi, T.S.; Que, D.L.; & Li, L.B. (1991). The evidence for interaction of the N-N pair with oxygen in Czochralski silicon. *J. Appl. Phys.*, Vol. 69, No. 6, pp. 3775-3777.
- Qi, M.W.; Shi, T.S.; Tan, S.S.; Zhu, B.; Cai, P.X.; Liu, L.Q.; Que D.L.; & Li, L.B. (1992). On the Determination of Nitrogen in Czochralski Silicon. *Materials Science Forum*, Vols. 83-87, pp. 263-268.
- Quast, F.; Pichler, P.; Ryssel, H.; & Falster, R. (2000). Vacancy-Nitrogen complexes in float-zone silicon. *Electrochemical Society Proceedings, High Purity Silicon VI*, Vols. 2000-17, pp. 156-163.
- Rozgonyi, G. A. ; Karoui, A.; Kvit, A.; & Duscher , G. (2002). Nano-scale analysis of precipitates in nitrogen-doped Czochralski silicon. *Microelectronic Engineering*, Vol. 66, No. 1-4, pp. 305-313.
- Sahtout Karoui, F. ; Karoui, A.; Rozgonyi, G. A.; Hourai, M.; & Sueoka, K. (2004). Characterization of Nucleation Sites in Nitrogen Doped Czochralski Silicon by Density Functional Theory and Molecular Mechanics. *Solid State Phenomena*, Vol. 95-96, pp. 99-104.
- Sawada, H.; & Kawakami, K. (2000). First-principles calculation of the interaction between nitrogen atoms and vacancies in silicon. *Phys. Rev. B*, Vol. 62, No. 3, pp. 1851-1858.

- Schultz, P.A. ; & Nelson, J.S. (2001). Fast through-bond diffusion of nitrogen in silicon. *Applied Physics Letters*, Vol. 78, No. 6, pp. 736-738.
- Shaik Adam, L.; Law, M. E.; Szpala, S.; Simpson, P.J.; Lawther, D.; Dokumaci, O. ; & Hegde, S. (2001). Experimental identification of nitrogen-vacancy complexes in nitrogen implanted silicon. *Applied Physics Letters*, Vol. 79, No. 5, pp. 623-625.
- Shimura, F.; & Hockett, R. S. (1986). Nitrogen effect on oxygen precipitation in Czochralski silicon. *Applied Physics Letters*, Vol. 48, No. 3, pp. 224-226.
- Stein, H. J. (1983). Vibrational absorption bands for implanted nitrogen in crystalline silicon. *Applied Physics Letter*, Vol. 43, No. 3, 296-298.
- Stein, H. J. (1986). Nitrogen in Crystalline Si. *Mat. Res. Soc. Symp. Proc.*, Vol. 59, 523-535.
- Stein, H. J. (1987). Nitrogen Related Donors in Silicon. *J. Electrochem. Soc.*, Vol. 134, No. 10, pp. 2592-2596.
- Stein, H. J. (1985). Infrared absorption band for substitutional nitrogen in silicon. *Appl. Phys. Lett.*, 47 (12), pp. 1339-1341.
- Sumino, K.; Yonenaga, I.; & Imai, M. (1983). Effects of nitrogen on dislocation behavior and mechanical strength in silicon crystals, *J. App. Phys.*, Vol. 54, No.4, pp. 5016-5020.
- Sun, Q.; Yao, K. H.; Gatos, H. C. ; & Lagowski, J. (1992). Effects of nitrogen on oxygen precipitation in silicon. *J. Appl. Phys.*, Vol. 71, No. 8, pp. 3760-3765.
- Takahashi, Jun; Nakai, Katsuhiko; Kawakami, Kazuto; Inoue, Yoshiharu; Yokota, Hideki; Tachikawa, Akiyoshi; Ikari, Atsushi; & Ohashi, Wataru (2003). Microvoid Defects in Nitrogen- and/or Carbon-doped Czochralski-grown Silicon Crystals. *Jpn. J. Appl. Phys.*, Vol. 42, No. 2A, pp. 363-370.
- Tamatsuka, M.; Kobayashi, N.; Tobe, S.; & Masui, T. (1999). High performance silicon wafer with wide grown-in void free zone and high density internal gettering site achieved via rapid crystal growth with nitrogen doping and high temperature hydrogen and/or argon annealing. *ECS. Proceedings, Defects in Silicon III*, Pennington N. J., 1999, Vol. 99-1, pp. 456-467.
- Umerski A.; & Jones, R. (1993). The interaction of oxygen with dislocation cores in silicon. *Philosophical Magazine A*, 67(4), 905-915.
- UniChem Software, Oxford Molecular Group, Inc.
- Von . Ammon, W.; Dreier, P.; Hensel, W.; Lambert, U.; & Koster, L. (1996). Influence of oxygen and nitrogen on point defect aggregation in silicon single crystals, *Materials Science and Engineering B*, Vol. 36, No. 1-3, pp. 33-41.
- Von Ammon, W.; Holzl, R.; Virbulis, J.; Dornberger, E.; Schmolke, R.; & Graf, D. (2001). The impact of nitrogen on the defect aggregation in silicon, *J. of Crystal Growth*, Vol. 226, pp. 19-30.
- Vosko, S. H. ; Wilk, L.; & Nusair, M. (1980). Accurate spin-dependent electron liquid correlation energies for local spin density calculations: a critical analysis. *Canadian Journal of Physics*, Vol.58, No. 8, pp. 1200-1211.
- Wagner, P. ; Oeder, R.; & Zulehner, W. (1988). Nitrogen-oxygen complexes in Czochralski-silicon. *Appl. Phys. A*, Vol. 46, No. 2, pp. 73-76.
- Watkins G. D.; & Corbett, J. W. (1965). Defects in Irradiated Silicon: Electron Paramagnetic Resonance of the Divacancy. *Phys. Rev.*, Vol. 138, No. 2A, pp. A543-A555.
- Whalley, E. (1972). The Dipole Moment Derivative of the Hydrogen Bond in Ice. *Canadian Journal of Chemistry*, Vol. 50, No. 3, pp. 310-314.
- Yang, D. ; Que, D.; & Sumino, K. (1998). Nitrogen-Oxygen Complexes in Silicon. *Phys. Stat. Sol. B*, Vol. 210, No. 2, pp. 295-299.



Some Applications of Quantum Mechanics

Edited by Prof. Mohammad Reza Pahlavani

ISBN 978-953-51-0059-1

Hard cover, 424 pages

Publisher InTech

Published online 22, February, 2012

Published in print edition February, 2012

Quantum mechanics, shortly after invention, obtained applications in different area of human knowledge. Perhaps, the most attractive feature of quantum mechanics is its applications in such diverse area as, astrophysics, nuclear physics, atomic and molecular spectroscopy, solid state physics and nanotechnology, crystallography, chemistry, biotechnology, information theory, electronic engineering... This book is the result of an international attempt written by invited authors from over the world to response daily growing needs in this area. We do not believe that this book can cover all area of application of quantum mechanics but wish to be a good reference for graduate students and researchers.

How to reference

In order to correctly reference this scholarly work, feel free to copy and paste the following:

Faouzia Sahtout Karoui and Abdennaceur Karoui (2012). Application of Quantum Mechanics for Computing the Vibrational Spectra of Nitrogen Complexes in Silicon Nanomaterials, Some Applications of Quantum Mechanics, Prof. Mohammad Reza Pahlavani (Ed.), ISBN: 978-953-51-0059-1, InTech, Available from: <http://www.intechopen.com/books/some-applications-of-quantum-mechanics/application-of-quantum-mechanics-for-computing-the-vibrational-spectra-of-nitrogen-complexes-in-sili>

INTECH
open science | open minds

InTech Europe

University Campus STeP Ri
Slavka Krautzeka 83/A
51000 Rijeka, Croatia
Phone: +385 (51) 770 447
Fax: +385 (51) 686 166
www.intechopen.com

InTech China

Unit 405, Office Block, Hotel Equatorial Shanghai
No.65, Yan An Road (West), Shanghai, 200040, China
中国上海市延安西路65号上海国际贵都大饭店办公楼405单元
Phone: +86-21-62489820
Fax: +86-21-62489821

© 2012 The Author(s). Licensee IntechOpen. This is an open access article distributed under the terms of the [Creative Commons Attribution 3.0 License](#), which permits unrestricted use, distribution, and reproduction in any medium, provided the original work is properly cited.

IntechOpen

IntechOpen